5 EFFECT OF ORIENTATION ON THE TENSILE PROPERTIES OF PLANT YARN REINFORCED COMPOSITES*

5.1 Introduction

Fibre reinforced plastics (FRPs) typically exhibit anisotropy. That is, some material properties are a function of the geometric axis/plane along which the properties are measured. The anisotropy of FRPs is a direct result of the dependency of composite mechanical properties on the orientation of the fibre reinforcement.

Current applications of plant fibre composites (PFRPs) are primarily based on compression moulded and injection moulded non-structural components for the automotive industry and consumer goods market [1]. The reinforcement is typically in the form of non-woven mats (for compression moulding) or granules/pellets (for injection moulding) [1, 2]. Employing discontinuous fibres in both cases, fibre orientation is 2D-random in the former and 3D-random in the latter. Due to the random orientation of the reinforcement, the resulting PFRP may have quasi-isotropic (for 2D-random) or even isotropic (for 3D-random) properties. However, the random fibre orientation implies that the reinforcement efficiency is severely compromised. According to Krenchel's reinforcement orientation efficiency factor [3], employing randomly oriented fibres in 2D or 3D reduces the reinforcing effect of the fibre (in terms of providing strength and stiffness) to 37.5% and 20.0% of its potential, respectively. For load-bearing applications, the use of reinforcements in the form of continuous aligned fibres is essential as they preserve high efficiency factors

Shah DU, Schubel PJ, Clifford MJ. Modelling the effect of yarn twist on the tensile strength of unidirectional plant fibre yarn composites. *Journal of Composite Materials*, 2012, 47(4): p. 425-436.

Shah DU, Schubel PJ, Clifford MJ, Licence P. The tensile behavior of off-axis loaded plant fiber composites: an insight on the non-linear stress-strain response. *Polymer Composites*, 2012, 33(9): p. 1494-1504.

DU Shah Page | 121

^{*} This chapter is based on the peer-reviewed journal articles:

(of length and orientation), thus allowing the entire properties of the fibre to be exploited. This was highlighted through the literature survey in *Chapter 2*.

Table 5.1 presents typically reported tensile properties of PFRPs and the unreinforced matrix. In particular, it highlights the difference in magnitude of the tensile properties for PFRPs reinforced with fibres in 3D-random, 2D-random and uniaxial orientation. The results reveal that PFRPs with random fibre orientation posses poor tensile properties with stiffness below 8 GPa and ultimate stress below 70 MPa. In fact, the tensile strength of the PFRPs is of similar order to that of the matrix. If the fibres are aligned, the (longitudinal) tensile properties are considerably improved. In addition, as highlighted in *Chapter 4*, aligned PFRPs have a lower minimum and critical fibre volume fraction and a higher maximum fibre volume fraction, than random fibre PFRPs [4, 5].

Table 5.1. Typically reported tensile properties of PFRPs with different fibre orientations.

Composite	Fibre content [%]	Fibre orientation	Testing direction	Tensile modulus [GPa]	Tensile strength [MPa]	Source
Epoxy	-	-	-	3.2	75	
Flax/epoxy	22 v	2D-Random	-	7.9	53	[6]
Flax/epoxy	48 v	Unidirectional	Longitudinal	32.0	268	[7]
Flax/epoxy	48 v	Unidirectional	Transverse	4.0	18	[7]
PP	-	-	-	1.7	28	[8]
Hemp/PP	30 wt	3D-random	-	1.5	30	[9]
Hemp/PP	40 wt	2D-Random	-	3.5	40	[10]
Hemp/PET	30 v	Unidirectional	Longitudinal	17.6	205	[8]
Hemp/PET	30 v	Unidirectional	Transverse	3.5	19	[8]

It should be noted that the transverse tensile properties of unidirectional PFRPs are low due to the anisotropy of the fibre and composite. However, this is often an advantage in structural applications, where the composite anisotropy can be deliberately aligned along a particular direction that is known to be the principally loaded axis/plane. For instance, uniaxial reinforcements are employed along the spar

of a wind turbine blade to resist axial/centrifugal loads. If necessary, multiple plies aligned in different directions (*i.e.* multi-axial reinforcements) can be used to resist off-axis and shear loads. In fact, some plies, in the form of biax $[\pm 45^{\circ}]$ and triax $[0,\pm 45^{\circ}]$, are employed in the blade spar and skin/shell, aligned off-axis to the leading edge, to resist shear loads related to torsion.

5.1.1 Misorientation in aligned PFRPs

Previously, the effect of orientation (in terms of random and aligned fibre orientation) on PFRP mechanical properties was discussed. However, in aligned PFRPs, (mis)orientation manifests itself in various other forms, at every length scale (Fig. 5.1): *a)* microfibril angle in a single plant fibre, *b)* twist angle in a processed staple fibre yarn, and *c)* off-axis loading angle in a composite laminate. Importantly, these misorientations play a major role in determining the mechanical properties of plant fibres and their composites.

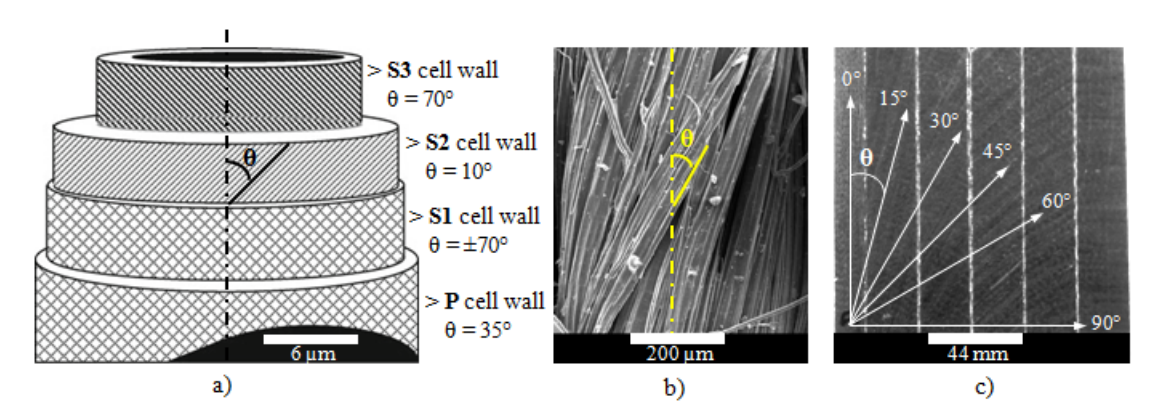


Fig. 5.1. The forms of misorientation: a) in the primary (P) and secondary (S) cell walls of a single flax fibre, cellulose microfibrils are oriented at an angle to the fibre axis [11]; b) in a staple fibre flax yarn, twisted fibres are located helically around the yarn axis; c) in a composite laminate, plies may be off-axis to the loading direction.

In this chapter, the effect of (mis)orientation on the mechanical behaviour of aligned PFRPs is investigated. In particular, this chapter aims to *i*) review the effect of the microfibril angle on the tensile properties of plant fibres, *ii*) model the effect of reinforcing yarn twist on PFRP tensile properties, and *iii*) evaluate the effect of offaxis loads on PFRP tensile properties. This will *i*) provide an improved

understanding on the mechanical behaviour and response of PFRPs, *ii*) enable the design and optimisation of PFRPs, and *iii*) enable the development of models to predict the mechanical properties of PFRPs. All of these are key to the employment of PFRPs for load-bearing applications.

5.2 THE MICROFIBRIL ANGLE IN PLANT FIBRES

Plant fibres themselves are composites containing cellulose microfibrils which are embedded in a lignin-hemicellulose matrix. Cellulose, the primary constituent of plant fibres, is highly anisotropic in crystalline form. In bast fibres like flax and hemp, cellulose crystallinity can be as high as 70% [12]. While extensive hydrogen bonding leads to a crystalline structure with a theoretical stiffness of 138-250 GPa in the chain direction, the molecular linearity of crystalline cellulose results in a transverse stiffness of only 15-30 GPa [13-19]. Furthermore, the cellulose microfibrils are helically wound around layers of cell walls (Fig. 5.1a) and hence they are not perfectly aligned but are at an angle to the fibre axis. Different layers of cell walls have a different microfibril angle [12, 19]. As the S2 cell wall accounts for more than 80% of the total cell wall thickness [12, 17], it is the microfibril angle (MFA) of the S2 cell wall that is of interest.

The role and effect of MFA on plant fibre tensile properties and stress-strain behaviour has been studied thoroughly by several researchers (for instance, [20] and references therein). The conclusions suggest that alongside the cellulose content of plant fibres, the MFA has a direct contribution to the mechanical properties of plant fibres [19, 21-27]. As Fig. 5.2 depicts, while plant fibre tensile modulus and strength are higher for lower MFA, the failure strain is smaller for lower MFA. In addition, the MFA also dictates the non-linear stress-strain behaviour of plant fibres [21, 23, 26, 28]; while the elastic range is smaller for higher MFA, the plastic range increases with increasing MFA (Fig. 5.2). Suslov *et al.* [29] report that even the mechanical anisotropy of plant seed fibres is dependent on the microfibril orientation.

In fact, the MFA of the S2 cell wall has such a dominating effect on plant fibre tensile properties that it can be used as a parameter to classify plant fibres into different categories. For instance, bast fibres are obtained from the inner bark of

dicotyledonous plants and provide structural strength, stiffness and rigidity to the plant stem. Hence bast fibres, such as flax, hemp and jute, have small MFA (<10°) [13, 30]. Leaf fibres are obtained from the leaves of monocotyledonous plants and provide them with the toughness and ductility required to withstand repetitive flexing motion in windy conditions. Hence leaf fibres, such as sisal, pineapple and banana, have moderate MFA (10–25°) [13, 30]. In seed fibres, like coir, cotton and oil palm, the cellulose microfibrils do not have any structural role and thus seed fibres have a high MFA (>25°) [13, 30]. Although orientation in plant fibres (MFA) cannot be actively controlled [31], it can be used as an indicator for potential applications of PFRPs made from a particular plant fibre.

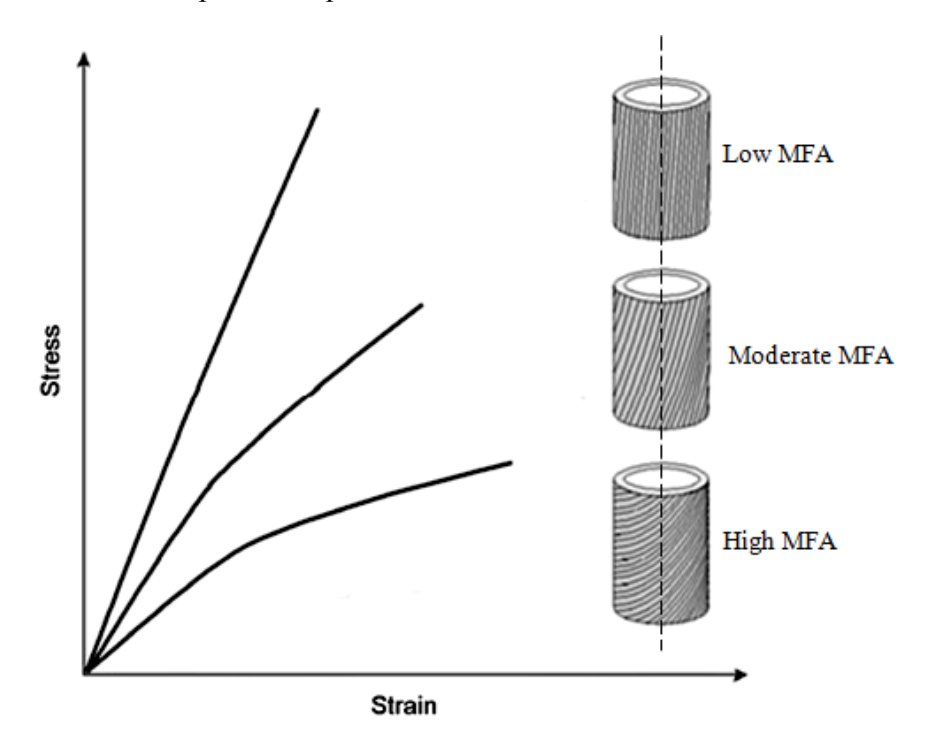


Fig. 5.2. Schematic tensile stress-strain curves of plant fibres showing the influence of MFA. A higher MFA leads to *i*) reduced elastic range, *ii*) reduced elastic modulus, *iii*) reduced tensile strength, *iv*) increased failure strain and *v*) increased non-linear elastic stress-strain response. Adapted from [26].

5.3 EFFECT OF YARN TWIST ON PFRP TENSILE STRENGTH

5.3.1 Twisted yarns as reinforcements

The true structural potential of plant fibres as reinforcing agents can only be realized when the highest reinforcement efficiency is employed. Hence, aligned unidirectional PFRPs are of interest. The manufacture of aligned PFRPs requires the reinforcement to be continuous. Due to the discontinuous length of technical plant fibres, staple fibre yarns – the most readily available 'continuous' plant fibre semi-products – need to be employed. Plant fibre yarns, whose primary application is found in textiles, are conventionally produced through ring-spinning. The spinning process gives the yarn a twisted structure, where twist is the primary binding mechanism. Twist induces inter-fibre friction and thus imparts processability to the yarn. The addition of twist in yarns affects the stress transfer between fibres within the yarn and thus influences both i) the strength of the yarn and the ii) fracture mechanism of the yarn (Fig. 5.3). In the textile industry, twist is defined by i) twist direction (S or Z), ii) twist level, T (tpm) and iii) twist multiplier, TM (= $T\sqrt{tex}$).

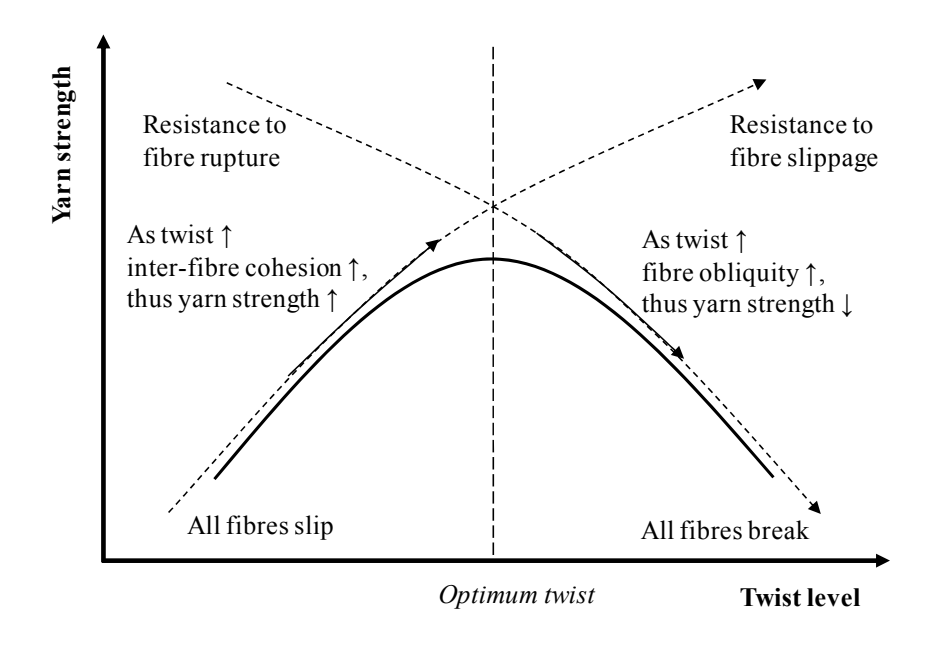


Fig. 5.3. The effect of twist on yarn tensile strength and failure mechanism. Up to a point, increasing twist level improves inter-fibre friction leading to an increase in yarn strength, after which fibre obliquity effects are significant leading to a drop in yarn strength.

Although twist is essential in the production of processable staple yarns and thus aligned PFRPs, there are significant detrimental effects on PFRP performance that need to be considered. Firstly, spinning plant fibres to form yarns is a costly and energy intensive process [32]. The price of flax yarns (and rovings) can be as much as 15 €/kg; this is over 10 times higher than the price of short technical flax fibres which cost between 0.5-1.5 \notin /kg [5, 30]. Finn *et al.* showed that the twist level T is inversely proportional to the production rate of a yarn and thus directly proportional to the cost of yarn spinning [33]. Hence, plant fibres would no longer be a low-cost substitute to E-glass. Secondly, when twisted yarns are used to produce woven textile reinforcements they cause 'crimp' which has a detrimental effect on composite properties due to yarn misalignments and resulting stress concentrations [34]. Thirdly, twist tightens the yarn structure which reduces yarn permeability and hinders yarn impregnation [35]. The hindered impregnation has shown to result in impregnation-related voids in PFRPs produced from twisted yarns (Chapters 3 and 4). Furthermore, the twisted nature of such textile plant fibre yarns leads to loss in reinforcement orientation efficiency despite laying the yarns as a unidirectional mat. Goutianos et al. [36] observed that the tensile strength of epoxy-impregnated twisted flax yarns (the simplest unidirectional PFRP) decreased with twist, similar to an offaxis loaded laminate; high-twist (~200 tpm) impregnated yarns show a drop in tensile strength by up to 70% when compared to low-twist (\sim 50 tpm) impregnated yarns.

There have been efforts to achieve full utilisation of the fibre properties in the final composite by reducing or replacing twist in yarns. Goutianos *et al.* [36] attempted to employ flax yarns with the minimal level of twist (~50 tpm) allowed by yarn processing requirements to produce aligned composites. Some European textile spinning companies are slowly coming to pace with the use of plant fibres for composites and are now producing rovings with insignificant twist levels (20 tpm), although not reduced prices. The author of this thesis has used such rovings (in the form of F20 in *Chapter 3*) for aligned thermoset composites and observed that the back-calculated flax fibre tensile modulus and specific tensile strength were comparable to that of E-glass. Baets *et al.* [37] have looked at the tensile properties of composites produced from flax fibres from different steps in the fibre extraction

and yarn preparation process. They observe that each stage increases the level of twist in the reinforcing fibres and although the dry bundle strength increases, composite properties are highest for minimally-processed hackled flax slivers with no twist. Zhang *et al.* [38] investigated the use of wrap-spinning to produce twist-less reinforcing fibres (wrapped by polypropylene, for instance) for reinforcement purposes. Although they observe a 7-30% higher flexural modulus for wrap-spun flax/PP composites, the flexural strength of wrap-spun flax/PP composites is similar to that of twisted yarn flax/PP composites.

5.3.2 Modelling the effect of twist on composite mechanical properties

As ring-spinning is the traditional method of producing yarns, twisted plant fibre yarns will remain the readily available form of textile reinforcements for PFRPs. Hence, modelling the effect of yarn twist on composite mechanical properties is essential for: *i)* appreciating the reduction in properties when twisted yarn reinforcements are used, and *ii)* estimating the potential composite properties if untwisted reinforcements were used.

There are no existing models to accurately predict the effect of yarn twist on composite tensile strength. Although there has been a recent interest in this topic by Ma *et al.* [39], their study considered only three different twist levels (0, 20 and 50 tpm). Twisted ring-spun yarns have a typical twist level of 150-200 tpm. In addition, the model Ma *et al.* [39] developed, doesn't consider structure-property relationships in a twisted staple fibre yarn and its effect on composite tensile strength.

However, some work (for instance, [40-42]) has been done on modelling the effect of yarn twist on the elastic properties (specifically, tensile modulus E) of high-performance and high-modulus synthetic impregnated filament yarns. The models of Rao *et al.* [40] and Naik *et al.* [41] to estimate impregnated yarn tensile modulus are comprehensive and take into account the effect of anisotropy, fibre migration, and micro-buckling. However, these models are complex, sophisticated and require the input of several material constants (including E_x , $E_y = E_z$, $G_{xy} = G_{xz}$, G_{yz} , $v_{xy} = v_{xz}$ and v_{yz}) which is cumbersome.

Baets *et al.* [37, 43] conducted a study to observe the evolution of the tensile modulus of unidirectional flax/epoxy composites with changing yarn twist levels. Interestingly, they found good agreement between their experimental data and the predictive models by Rao *et al.* [40] and Naik *et al.* [41]. In another study, Rask *et al.* [44] found no correlation between yarn twist level and uniaxial PFRP tensile modulus. However, it should be noted that Rask *et al.* [44] were employing wrapspun yarn, as opposed to ring-spun yarn.

There has been no direct study on the effect of yarn twist on composite tensile strength, let alone PFRP tensile strength. This study looks at providing a simple, yet accurate model for the effect of yarn twist on unidirectional tensile strength of PFRPs. The model is validated by extensive experimental data from Goutianos *et al.* [36] showing a near-perfect R²-value (from non-linear regression) of 0.950. Data from Baets *et al.* [37, 43] is also used to further verify the developed model.

5.3.3 Structure of a twisted staple yarn

To develop an effective model of unidirectional composite tensile strength of PFRPs reinforced with staple yarns, the structure of a staple yarn needs to be defined.

The effect of twist angle of a continuous filament yarn on the dry yarn tensile modulus was investigated as early as 1907 by Gegauff [45] and then by Platt [46]. The simplest, and widely accepted, structure of a filament yarn was proposed as the ideal coaxial model. Staple fibre yarns are structurally more complex than filament yarns. Filament yarns are more uniform in terms of i) fibre distribution (packing fraction \emptyset), ii) fibre configuration within the yarn (small fibre migration) and iii) yarn mechanical properties (as the single filaments have uniform properties). In staple yarns, the packing fraction is a function of yarn radius (the centre being more densely packed) and fibre migration is more important due to the short length of the individual fibres. Furthermore, plant fibres have variable physical and mechanical properties, which translate into the staple fibre yarn as well; that is, the fibres do not break at the same time in a staple yarn.

The yarn in this study is assumed to be the so-called idealized staple fibre yarn (as defined by Hearle et al. [47]). In such a yarn, whose cross-section is circular with

radius r (Fig. 5.4), the twist angle θ_x of an arbitrary fibre at a radial position x ($0 \le x \le r$) is given by

$$\tan \theta_x = \frac{2\pi x}{L}$$
 Eq. 5.1

The twist angle at the yarn surface α (at radius r, $\alpha = \theta_r$) can be defined in terms of the twist level T = 1/L), as in Eq. 5.2, where L is the length of the yarn for one turn.

$$\tan \alpha = \frac{2\pi r}{L} = 2\pi rT$$
 Eq. 5.2

The yarn packing fraction \emptyset is the ratio of the true fibre cross-sectional area A_f to the yarn cross-sectional area A_v and can be written as

$$\phi = \frac{A_f}{A_v} = \frac{\overline{\rho}}{\pi \rho r^2}$$
 Eq. 5.3

where, ρ is the fibre density and $\overline{\rho}$ is the yarn mass per unit length (= $10^{-6} \times tex$).

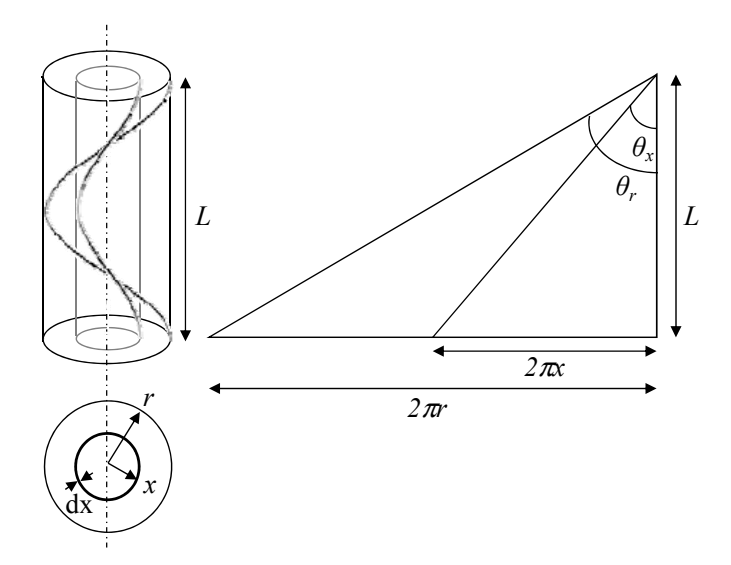


Fig. 5.4. Idealized structure of a twisted staple fibre yarn.

As PFRP misalignment or orientation efficiency would be a function of fibre orientation, Eq. 5.2 and Eq. 5.3 are rearranged to calculate the surface twist angle α for known values of twist level T, yarn linear density tex, fibre density ρ and packing fraction \emptyset .

$$\alpha = \tan^{-1} \left(10^{-3} \cdot T \sqrt{4\pi \cdot \frac{tex}{\rho \phi}} \right)$$
 Eq. 5.4

In the above yarn structure model, we adopt all the assumptions made by Hearle *et al.* [47] (*listed in Appendix C*) except that the yarn packing fraction \emptyset is no longer neglected (or assumed to be unity), but is allowed to change along with the yarn twist level. Pan [48] derived a semi-empirical equation to describe the relationship between packing fraction \emptyset and twist level T for staple fibre yarns (Eq. 4.5). In Eq. 4.5, \emptyset_{max} is the maximum packing fraction of the yarn, and A and B are constants.

$$\phi = \phi_{\text{max}} \left(1 - A e^{-BT} \right)$$
 Eq. 4.5

In *Chapter 4*, it was shown the packing fraction \emptyset of staple fibre yarns used for PFRPs is well described by Eq. 4.5 with the factors \emptyset_{max} , A and B of 0.6, 0.78 and 0.0195, respectively. The result of Eq. 4.5 is shown in Fig. 5.5. Fig. 5.5 also presents the effect of packing fraction on the curve of surface twist angle against twist level. It is observed that a constant yarn packing fraction of $\emptyset = 0.6$ approximates Eq. 5.4 well. This is useful as ring-spun yarns typically have a packing fraction of 0.5-0.6 [49].

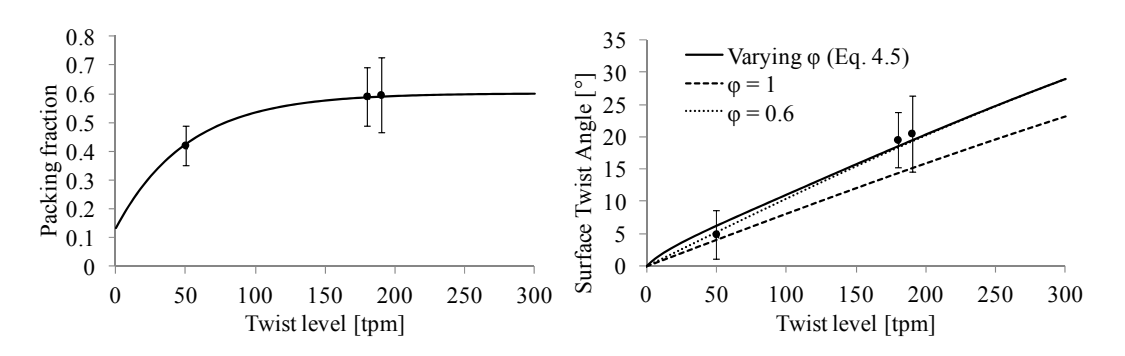


Fig. 5.5. The effect of twist level on packing fraction and yarn surface twist angle. Experimental data (from *Chapter 3 and Appendix A*) (\bullet) shows good agreement with yarn structure model.

The effect of yarn linear density on the curves of i) packing fraction versus surface twist angle and ii) surface twist angle versus twist level have been presented in Fig. 5.6. A fibre density of 1550 kgm⁻³ is assumed. It is observed that a heavier yarn

(higher tex) has a higher surface twist angle and lower packing fraction due to a larger yarn diameter.

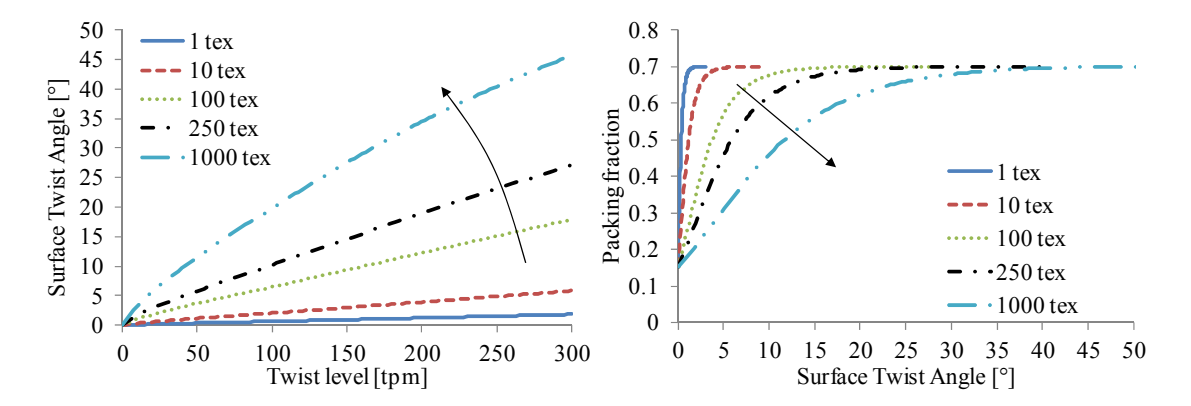


Fig. 5.6. The effect of increase yarn linear density (tex) on yarn structure.

Although the packing fraction is allowed to vary with twist level, the packing fraction within a yarn is assumed to be uniform for a given twist level. This structure of the idealized yarn model also assumes no fibre migration and no micro-buckling.

5.3.4 Experimental data

To validate the predictive models, experimental data from Goutianos *et al.* [36] has been used. To investigate the effect of twist on tensile strength of aligned composites, they used two different flax yarns: *i)* yarns made from long flax fibres (609 tex) and *ii)* yarns made from short flax fibres (1000 tex). The yarns were first impregnated in epoxy resin and then manually twisted to seven different twist levels (ranging from about 50 tpm to 250 tpm). Twisting of yarn after impregnation ensured that the effect of decreasing permeability with increasing twist was excluded, thus allowing a true study of the effect of twist alone. To examine the tensile strength of the impregnated yarns, they were tested in tension at a cross-head speed of 2 mm/min. They calculated the tensile strength using the yarn cross-sectional area.

As modelling the tensile strength of a twisted yarn composite is more convenient and geometrically sensible when twist is presented in terms of surface twist angle α rather than twist level T, the data from Goutianos *et al.* [36] has been translated in terms of surface twist angle (Fig. 5.7). To convert the twist level T to the surface twist angle

 α , Eq. 5.4 is used where the flax fibre density is taken to be 1550 kgm⁻³, the yarn linear density is taken to be 609 tex for long and 1000 tex for short flax fibre yarns, and the packing fraction \emptyset is calculated for different twist levels using Eq. 4.5. The results are graphically presented in Fig. 5.7. It is observed that short flax fibre yarns have a higher surface twist angle than long flax fibre yarns, despite having a lower twist level (tpm). This is because they are heavier (higher tex) and thus have a larger yarn diameter.

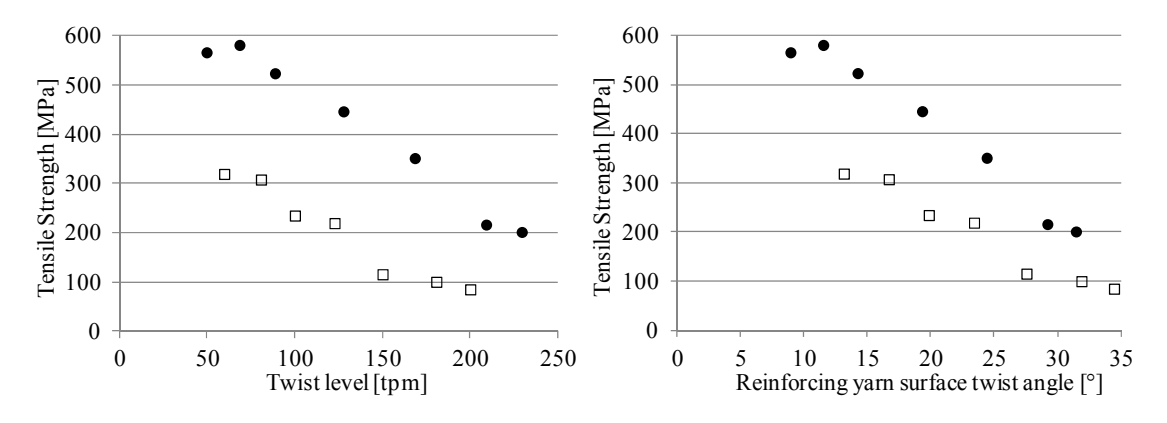


Fig. 5.7. Tensile strength of (\bullet) long and (\neg) short flax fibre epoxy impregnated yarns as a function of twist level (left) [36] and surface twist angle (right).

5.3.5 Mathematical models

5.3.5.1 Tsai-Hill composite laminate model

An impregnated yarn is fundamentally a composite material. In fact, it seems that a twisted impregnated plant fibre staple yarn is similar to an off-axis unidirectional laminate not only in geometry (as revealed in Fig. 5.8) but also in the way the tensile strength of the impregnated yarn drops with increasing twist (Fig. 5.7).

Hence, the simplest model would be based on an off-axis laminate. The uniaxial failure stress of an off-axis composite σ_{θ} can be estimated by the empirical Tsai-Hill failure criterion [50], which is defined by equation Eq. 5.5.

$$\sigma_{\theta} = \left[\frac{1}{\sigma_0^2} \cos^4 \theta + \left(\frac{1}{\tau^2} - \frac{1}{\sigma_0^2} \right) \cos^2 \theta \sin^2 \theta + \frac{1}{\sigma_{90}^2} \sin^4 \theta \right]^{-0.5}$$
 Eq. 5.5

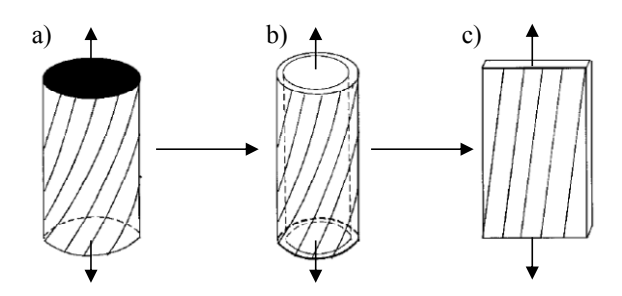


Fig. 5.8. An impregnated yarn is similar to an off-axis composite. a) twisted impregnated yarn with surface twist angle α , b) a layer of a twisted impregnated yarn, c) the open-up structure of the layer is a laminate with off-axis loading angle θ .

The Tsai-Hill criterion is suitable for idealised twisted staple fibre yarns and their unidirectional composites as they can be considered as transversely isotropic structures under plane stress conditions [40, 48]. From tests on the effect of loading angle on the uniaxial tensile strength of unidirectional flax/polyester composites (v_f = 27%) (*Chapter 3 and Chapter 5.6*), it has been found that the longitudinal tensile strength σ_0 is 7 times higher than the inter-laminar shear strength τ and 11 times higher than the transverse tensile strength σ_{90} so that

$$\frac{\sigma_0}{\tau} = 7; \ \frac{\sigma_0}{\sigma_{00}} = 11$$
 Eq. 5.6

Using Eq. 5.6 and trigonometric identities (specifically, $\cos^4\theta + 2\sin^2\theta\cos^2\theta + \sin^4\theta = 1$ and $\cos^2\theta = 1 - \sin^2\theta$) the Tsai-Hill criterion in Eq. 5.5 can be generalized as given in Eq. 5.7 to predict the composite tensile strength as a function of misorientation θ .

$$\sigma_{\theta} = \sigma_0 [1 + 46\sin^2\theta + 74\sin^4\theta]^{-0.5}$$
 Eq. 5.7

As the idealised yarn structure depicts (Section 5.3.3), the twist angle θ_x is a function of the yarn radius. The twist angle increases from 0 at the yarn centre to a maximum of α at the yarn surface. To incorporate the structure of the staple fibre yarn into the Tsai-Hill model, it is possible to define a mean twist angle θ_{mean} which can be then substituted into Eq. 5.7. Madsen *et al.* [51] have derived an expression for this mean twist angle θ_{mean} by integrating the proportional contribution of θ_x over $0 \le x \le r$ (Eq.

5.8). They find that θ_{mean} is conveniently a function of the surface twist angle α (Eq. 5.9).

$$\theta_{mean} = \int_{0}^{r} \frac{2\pi x}{\pi r^2} \tan^{-1} \left(\frac{2\pi x}{L}\right) dx$$
 Eq. 5.8

$$\theta_{mean} = \alpha + \frac{\alpha}{\tan^2 \alpha} - \frac{1}{\tan \alpha}$$
 Eq. 5.9

The Tsai-Hill criterion in Eq. 5.7 can be re-written for θ_{mean} (Eq. 5.10).

$$\sigma_{\theta=\theta_{mean}} = \sigma_0 \left[1 + 46 \sin^2 \theta_{mean} + 74 \sin^4 \theta_{mean} \right]^{-0.5}$$
 Eq. 5.10

Eq. 5.10 can be then used to apply the Tsai-Hill model onto the experimental data. This is presented graphically in Fig. 5.9 and Fig. 5.10. The best fit is given for a σ_0 of 670 MPa for long flax fibre impregnated yarns and 400 MPa for short flax fibre impregnated yarns. It is expected that the longitudinal tensile strength σ_0 will be smaller for short fibre composites.

An R²-value (non-linear regression) of 0.893 for long flax fibre impregnated yarns and 0.913 for short flax fibre impregnated yarns is observed. The high R²-values suggest that the Tsai-Hill model (accounting for yarn structure and geometry) is a reasonable fit to the experimental data. However, it can be graphically seen (Fig. 5.9 and Fig. 5.10) that the model does not accurately depict the variation of composite tensile strength with increasing yarn twist angle. None of the experimental datapoints lie on the curve. The Tsai-Hill model under-estimates the tensile strength of impregnated yarns for $\alpha < 27^{\circ}$ (or $\theta_{mean} > 18.5^{\circ}$) and over-predicts the tensile strength for $\alpha > 27^{\circ}$ (or $\theta_{mean} > 18.5^{\circ}$).

Although the Tsai-Hill criterion in Eq. 5.10 accounts for the yarn structure, it does not model the experimental data accurately possibly because incorrect stress ratios, σ_0/σ_{90} and σ_0/τ , may have been used. As the experimental data is based on impregnated yarns rather than true aligned composite laminates, the stress ratios that should be used should be based on the former rather than the latter. The Tsai-Hill criterion in Eq. 5.11 uses stress ratios that best fit the experimental data, giving an R²-value > 0.940. The stress ratios that have been used in Eq. 5.11 are $\sigma_0/\tau = 3.6$ and

 $\sigma_0/\sigma_{90}=22.6$. The physical implication of the best-fit stress ratios used in Eq. 5.11 is that best-fit interlaminar shear strength and best-fit transverse strength are double and half the values that were used in Eq. 5.6 and Eq. 5.10 (based on testing of aligned PFRP laminates). While the difference in stress ratios between impregnated yarns and composite laminates of plant fibres is large, it is not the case for synthetic fibre impregnated yarns and composite laminates. While σ_0/τ and σ_0/σ_{90} for epoxy impregnated T300/5208 carbon yarn ($v_f=0.7$) is 16.2 and 33.2, respectively, σ_0/τ and σ_0/σ_{90} for a unidirectional T300/5208 carbon/epoxy composite laminate ($v_f=0.7$) is 22.1 and 37.5, respectively [52]. In fact, it is surprising that while the estimated best-fit interlaminar shear strength of the flax/epoxy impregnated yarn ranges between $\tau=111-186$ MPa (depending on long or short flax fibres), the interlaminar shear strength of the T300/5208 carbon/epoxy impregnated yarn is much lower at 100-108 MPa. The reliability of the best-fit stress ratios and the applicability of Eq. 5.11 are thus questionable.

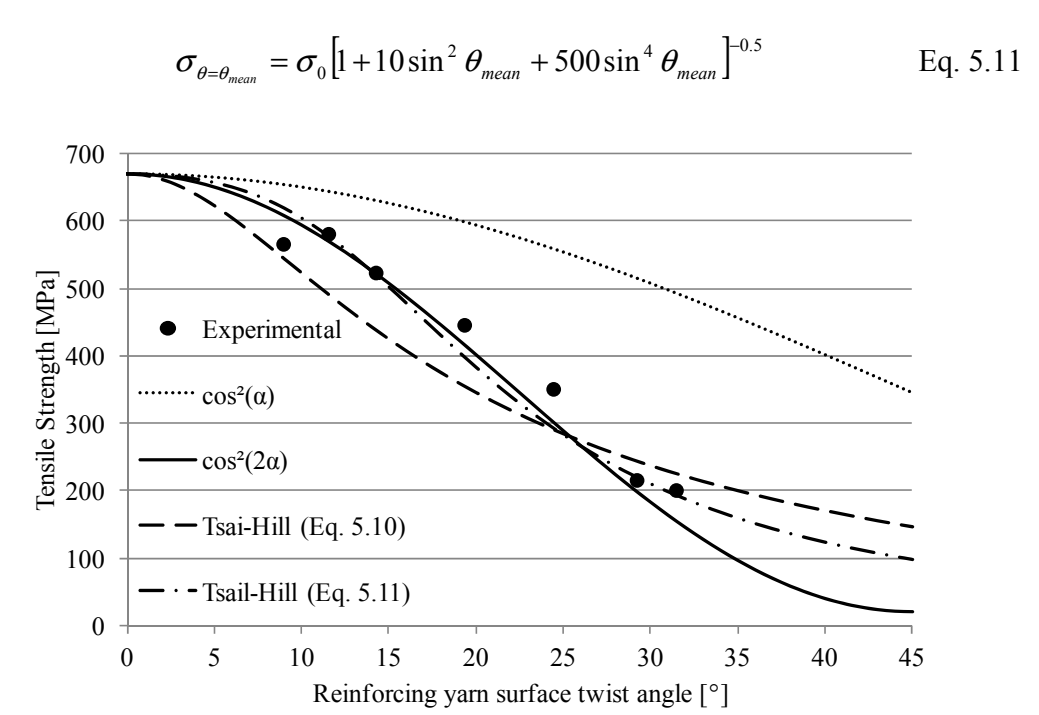


Fig. 5.9. Modelling the effect of yarn twist on long flax fibre impregnated yarn (unidirectional PFRP). The derived $\cos^2(2\alpha)$ model (based on Eq. 5.24) in this study provides best agreement with the experimental data with an R^2 -value of 0.950.

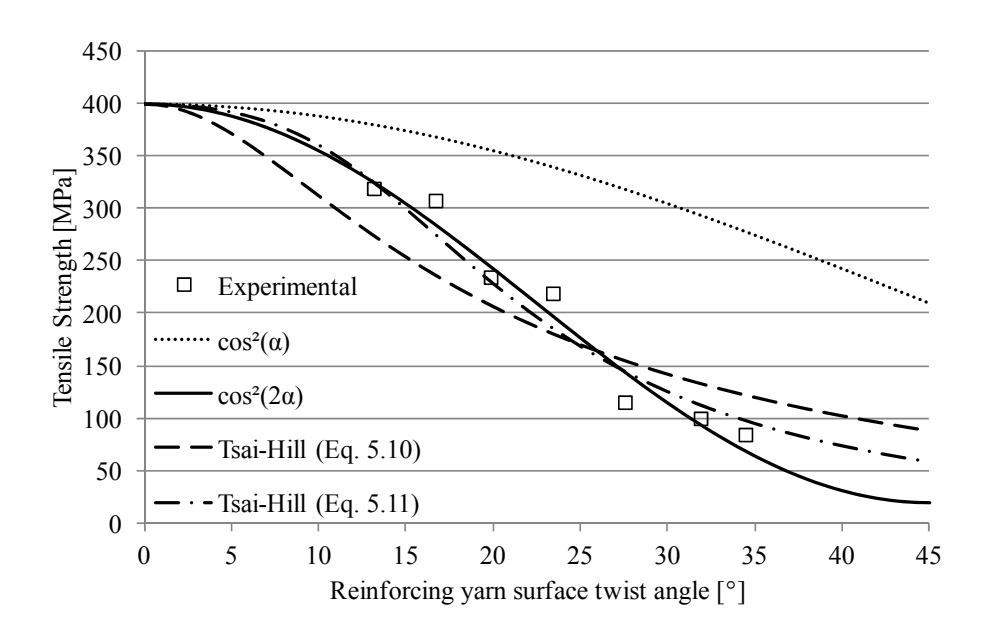


Fig. 5.10. Modelling the effect of yarn twist on short flax fibre impregnated yarn (unidirectional PFRP). The derived $\cos^2(2\alpha)$ model (based on Eq. 5.25) in this study provides best agreement with the experimental data with an R^2 -value of 0.961.

A limitation of the Tsai-Hill criterion is that it does not account for the non-uniform radial stress and strain distribution within an axially loaded impregnated yarn [53], and is solely dependent on the stress ratios. An alternate model is of interest.

5.3.5.2 Derived model: Krenchel efficiency factor for twisted yarns

The approach used here to model how the tensile strength of aligned PFRPs is influenced by the degree of twist is straightforward. This involves integrating the ideal twisted structure of a staple yarn into the Krenchel orientation efficiency factor and substituting the result into the rule of mixtures for composites to produce a mathematical model.

The rule of mixtures for PFRPs

The rule of mixtures for composites is the simplest and widely used model to describe variables that affect composite properties and parameters that account for the efficiency of the reinforcing fibres. As discussed in detail in *Chapter 2.4*, Summerscales *et al.* [54] have suggested a modified rule of mixtures for PFRPs with

efficiency terms that account for *i*) porosity v_p , *ii*) fibre length and interface η_{lS} , *iii*) fibre orientation distribution η_o , and *iv*) fibre diameter distribution η_d .

$$\sigma_c = (\eta_{IS} \eta_o \eta_d v_f \sigma_f + v_m \sigma'_m) (1 - v_p)^2$$
 Eq. 5.12

where σ'_m is defined as the matrix stress at fibre failure strain. To allow for the effect of fibre orientation distribution η_o on composite mechanical performance, typically the Krenchel orientation efficiency factor (Eq. 5.13) [3] can be calculated

$$\eta_o = \sum_n a_n \cos^4 \theta_n$$
 Eq. 5.13

where a_n is the fraction of fibre with orientation angle θ_n with respect to the axis of loading. These models assume iso-strain conditions, perfect fibre/matrix interface, elastic response of fibre and matrix, and no transverse deformations (ignore Poisson's effects).

Integrating the staple yarn structure into the Krenchel efficiency factor

A twisted staple fibre yarn, whose structure has been depicted in an earlier section (Fig. 5.4), is basically an induced misalignment of the fibres. The misalignment can be described in terms of the twist angle of the individual fibres θ_x within the yarn as a function of fibre radial position x ($0 \le x \le r$) using Eq. 5.1. This can then be integrated into the orientation efficiency factor of Eq. 5.13. The analysis is presented hence-forth.

As the spatial fibre distribution (packing fraction) in the yarn cross-section (of a given twist level) is assumed uniform and the radial location of a given fibre is fixed (that is, no fibre migration), a_n is given by Eq. 5.14. The values of a_n sum to unity.

$$a_n = \frac{2\pi x dx}{\pi r^2}$$
; $\int_0^r a_n = 1$ Eq. 5.14

From Eq. 5.1, Eq. 5.13 and Eq. 5.14, the Krenchel orientation efficiency factor η_o is then given by the integral

$$\eta_o = \int_0^r \frac{2\pi x}{\pi r^2} \cos^4 \left(\tan^{-1} \frac{2\pi x}{L} \right) dx$$
Eq. 5.15

Using the trigonometric identity $\cos^4(\tan^{-1}(u)) = 1/(1+u^2)^2$ to solve the integral in Eq. 5.15, results in an expression for the orientation efficiency factor η_o which is given in Eq. 5.16.

$$\eta_o = \frac{L^2}{L^2 + 4\pi^2 r^2}$$
 Eq. 5.16

Eq. 5.16 can be simplified using Eq. 5.2 to give Eq. 5.17. An expression for η_o (Eq. 5.17) is then found to be simply a function of the twist angle at the yarn surface α .

$$\eta_o = \frac{L^2}{L^2 + L^2 \tan^2 \alpha}$$
 Eq. 5.17

$$\eta_a = \cos^2 \alpha$$
 Eq. 5.18

When modelling the effect of fibre obliquity (yarn twist) on dry yarn tensile modulus, Pan [55] observed that a better agreement with experimental data was found when α is replaced with 2α . Pan [55] suggested that this is because the actual effect of the fibre helix angle is represented by 2α due to the structural difference between filament and staple yarns. However, the actual physical implication of the 2α in terms of the limiting twist angle for a staple yarn is not fully understood [55]. Filament yarns have a maximum permissible twist angle of 70.5° ; staple yarns will have a smaller limiting twist angle [47]. A factor of 2α restricts this limiting twist angle to 45° . Nonetheless, as Pan [55] observed better agreement with their experimental data, here the chosen model is based on 2α (Eq. 5.19) to predict the effect of twist on the tensile strength of aligned PFRPs.

$$\eta_a = \cos^2 2\alpha$$
 Eq. 5.19

Model for tensile strength prediction of twisted yarn PFRPs

The derived orientation efficiency factor (Eq. 5.19) needs to be substituted into the rule of mixtures for PFRPs (Eq. 5.12). The modified rule of mixtures which takes into account the effect of fibre obliquity in twisted yarn reinforcements is given by Eq. 5.20.

$$\sigma_c = (\cos^2 2\alpha \cdot \eta_{IS} \eta_d v_f \sigma_f + v_m \sigma_m^{\dagger}) (1 - v_p)^2$$
 Eq. 5.20

To compare the generalized model in Eq. 5.20 with the experimental data, some simplification is necessary. It is assumed that η_d is unity and that the composite contains no voids ($v_p = 0$ and $v_m = 1 - v_f$). The simplified model can be written as in Eq. 5.21

$$\sigma_{\alpha} = \cos^2 2\alpha \cdot \eta_{lS} v_f \sigma_f + (1 - v_f) \sigma'_m$$
 Eq. 5.21

As a side note, it is interesting that Eq. 5.21 is of similar form to that presented by McLaughlin *et al.* [21] to describe the effect of microfibril angle in single plant fibres on their elastic modulus (described in *Chapter 2*). A single plant fibre can be thought to be a twisted yarn composite; single plant fibres are a lignin-hemicellulose matrix reinforced by cellulose fibrils, where the microfibrils are helically wound around layers of the cell wall (previously described in Section 5.2).

Goutianos *et al.* [36] determined the tensile strength of the impregnated yarns using the cross-sectional area of the yarn. The cross-sectional area of a yarn is directly related to the yarn packing fraction (Eq. 5.3; $\emptyset = A_f/A_y$). Ring-spun yarns typically have a packing fraction of 0.5-0.6 [49]. As also discussed previously in Section 5.3.3, a constant packing fraction of $\emptyset = 0.6$ is a good match to Eq. 4.5. For an impregnated yarn, the yarn packing fraction \emptyset also represents the fibre volume fraction v_f . Hence, to compare the simplified model in Eq. 5.21 with the experimental data, the composite fibre volume fraction is taken to be $v_f = 0.6$. Other researchers, when modelling the elastic properties of impregnated twisted yarns, have also used a constant $v_f = 0.6$ [41]. Weyenberg *et al.* [7] calculated the matrix stress at fibre failure strain σ'_m (based on composite tensile strain of approximately 1.5%) of an epoxy matrix as $\sigma'_m = 50$ MPa.

The simplified model in Eq. 5.21 (with $v_f = 0.6$ and $\sigma'_m = 50$ MPa) can then be fitted to the experimental data for an adjusted effective fibre strength $\eta_{IS} \cdot \sigma_f$. The effective fibre strength $\eta_{IS} \cdot \sigma_f$ represents the potential reinforcing ability the fibres (of a given length) can provide to the composite. Typically, shorter fibres produce poorer composites due to smaller length efficiency factor η_{IS} and thus smaller effective fibre strength $\eta_{IS} \cdot \sigma_f$. The effective fibre strength is taken to be $\eta_{IS} \cdot \sigma_f = 1083$ MPa for long

flax fibres and η_{IS} $\sigma_f = 633$ MPa for short flax fibres. These values are in the range of typical tensile strength of technical flax fibres [30].

On a side note, if η_{lS} is assumed to be unity for long flax fibres (that is, $\sigma_f = 1083$ MPa), then $\eta_{lS} = 0.58$ for short flax fibres. The length efficiency factor η_{lS} is related to the critical (or ineffective) fibre length l_c (Eq. 5.22) [56], and l_c itself is defined by the composite interfacial shear strength τ , fibre strength σ_f and fibre diameter d_f (Eq. 5.23) [13, 56]. Hence, a value of $\eta_{lS} \approx 1$ implies that the reinforcing fibre length is significantly higher than the critical fibre length ($l_f > l_c$), while $\eta_{lS} = 0.58$ implies that the reinforcing fibre length is approximately equal to the critical fibre length ($l \approx l_c$).

$$\eta_{IS} = \begin{cases} 1 - l_c / 2l_f & for l_f \ge l_c \\ l_f / 2l_c & for l_f \le l_c \end{cases}$$
 Eq. 5.22

$$l_c = \frac{\sigma_f d_f}{2\tau}$$
 Eq. 5.23

In short, the derived mathematical models for the experimental data are given in Eq. 5.24 for long flax fibre impregnated yarn strength and Eq. 5.25 for short flax fibre impregnated yarn strength (where $v_f = 0.6$, $\sigma'_m = 50$ MPa and $\eta_{IS} \cdot \sigma_f = 1083$ MPa for long flax fibres and $\eta_{IS} \cdot \sigma_f = 633$ MPa for short flax fibres).

$$\sigma_{\alpha} = \cos^2 2\alpha \cdot 650 + 20$$
 Eq. 5.24

$$\sigma_{\alpha} = \cos^2 2\alpha \cdot 380 + 20$$
 Eq. 5.25

The $\cos^2(2\alpha)$ models have been compared with experimental data for long and short flax fibre yarns in Fig. 5.9 and Fig. 5.10. The $\cos^2(2\alpha)$ model is a near-perfect fit for the experimental data, where almost all the points lie on the curve. The non-linear regression R²-value is found to be 0.950 and 0.961 for long and short flax fibre impregnated yarns, respectively. A χ^2 -goodness of fit test suggests that the $\cos^2(2\alpha)$ is a suitable model for the experimental data at a p-value of 0.23% for the long flax impregnated yarns and at a p-value of 4.72% for the short flax impregnated yarns.

It is thus proposed that the simplified model in Eq. 5.21 is a good model to predict the influence of yarn twist on aligned PFRP tensile strength. If required, the other

efficiency factors and the effect of porosity can be reintroduced by using the generalized model in Eq. 5.20. An interesting inference of the model is that employing yarns with $\alpha > 26^{\circ}$ or $\alpha > 32^{\circ}$ as composite reinforcements will reduce the reinforcement orientation efficiency factor as in a 2D-random and 3D-random composite, respectively.

Applying the derived model to other studies

Although the derived model is in strong agreement with experimental data from Goutianos *et al.* [36], to validate the model further it is necessary to compare it with experimental results of real composites (rather than just impregnated yarns), from other studies.

Apart from Goutianos *et al.* [36], Baets *et al.* [37, 43] and Rask *et al.* [44] have investigated the effect of yarn twist on PFRP mechanical properties. As mentioned earlier, both Baets *et al.* [37, 43] and Rask *et al.* [44] focussed on the evolution of the tensile modulus of unidirectional composites for increasing yarn twist levels. Rask *et al.* [44] haven't presented data on composite tensile strength. Hence, the experimental data for Baets *et al.* [37, 43] has been used here.

Baets *et al.* [37, 43] manufactured unidirectional flax/epoxy composites from three different forms of flax: hackled, roving and yarn. Starting from the same source, the three different forms of flax were obtained from different steps in the fibre extraction and yarn preparation process. The key difference in them is their level of twist: 0 tpm, 41 tpm and 280 tpm, respectively. The corresponding surface twist angles were determined by Baets *et al.* [37, 43] and are presented in Table 5.2.

Baets *et al.* [37, 43] measured the tensile strength of the three UD composites. The experimental data is presented in Table 5.2. They determined the fibre tensile strength σ_f through back-calculation from the rule of mixtures – using Eq. 5.21, with the corresponding v_f and assuming $\eta_{IS}=1$ and $\sigma'_m=40$ MPa. They also assumed $\eta_o=1$ and consequently didn't consider the effect of (mis)orientation from increasing twist angle. What they observed is that the back-calculated single fibre tensile strength decreased with increasing twist level (Table 5.2). For instance, flax fibres from the yarn ($\alpha=14.8^{\circ}$) have a mean tensile strength of 590 MPa, which is 30%

lower than the mean tensile strength of flax fibres from a hackled bundle ($\alpha = 0^{\circ}$). The difference in mean tensile strength of the three flax fibres is accountable to the level of twist in the reinforcement type.

Table 5.2. Verification of the developed model with experimental data from Baets *et al.* [37, 43] (with column titles in italics).

	Fibre properties	Composite properties			Fibre tensile strength σ_f $\left[\mathrm{MPa} \right]^*$	
	Surface	Fibre	Tensile			
Flax	twist angle	content	Strength	2	For	For
type	α [°]	v_f	σ [MPa]	$\cos^2(2\alpha)$	$\eta_o = 1^{\dagger}$	$\eta_o = \cos^2(2\alpha)^{\ddagger}$
Hackled	0	42 ± 2	378 ± 38	1.000	845 ± 90	845 ± 90
Roving	7.8	48 ± 1	377 ± 24	0.928	742 ± 50	800 ± 54
Yarn	14.8	50 ± 1	315 ± 46	0.607	590 ± 92	780 ± 151

^{*} The fibre tensile strength is back-calculated using the rule of mixtures in Eq. 5.21, assuming $\eta_{IS} = 1$ and $\sigma'_m = 40$ MPa [11, 21].

Hence, to assess the validity of the model derived in the previous section, rather than assuming η_o to be unity, $\eta_o = \cos^2(2\alpha)$ is used in Eq. 5.21. The back-calculated fibre tensile strength will now account for misorientation from yarn twist. As can be seen in Table 5.2, the fibre tensile strengths are now very similar and in the range of 780–845 MPa; a difference of means t-test suggests an insignificant difference in the mean fibre tensile strengths (p>0.35). This shows that both the derived model and the $\cos^2(2\alpha)$ orientation efficiency factor are able to capture the effect of yarn twist on composite tensile strength.

5.3.6 Conclusions

The true structural potential of plant fibres as reinforcing agents can only be realized when the highest reinforcement efficiency is employed. Hence, aligned unidirectional PFRPs are of interest. However, due to the short length of technical plant fibres, the manufacture of aligned PFRPs requires the reinforcement to be in the

[†] Baets *et al.* [11, 21] determined the fibre tensile strength assuming no effect of (mis)orientation from yarn twist (that is, $\eta_o = 1$). The back-calculated fibre strengths are hence very dissimilar.

[‡] Using $\eta_o = \cos^2(2\alpha)$ in Eq. 5.21 accounts for the effect of yarn twist. The back-calculated fibre strengths are now similar to each other.

form of staple fibre yarns. Staple fibre yarns have a twisted structure. Although twist facilitates yarn processability, it has several detrimental effects on the composites produced from such twisted yarn reinforcements. One of these detrimental effects is fibre obliquity and misalignment (to the composite loading axis) which results in a drastic drop in mechanical properties of the composite.

Prior to this investigation, no analytical model was available to accurately predict the effect of yarn twist on aligned PFRP tensile strength. In this study, a novel mathematical model based on *i*) the modified rule of mixtures for PFRPs, *ii*) idealised twisted structure of a staple fibre yarn, and *iii*) Krenchel orientation efficiency factor is used to predict the influence of yarn twist on composite strength. The simple model is based on the yarn surface twist angle α . Through a discussion of the idealized staple yarn structure, relationships between structure and properties have been identified. A rule of mixtures model with a modified orientation efficiency factor of $\cos^2(2\alpha)$ is validated with extensive experimental data from Goutinos *et al.* [36] and shows strong agreement. The derived model is a near-perfect fit for the experimental data (with $R^2 = 0.950$). The model is verified further using experimental data from another study on aligned PFRPs by Baets *et al.* [37, 43]. An interesting inference of the model is that employing yarns with $\alpha > 26^{\circ}$ or $\alpha > 32^{\circ}$ as composite reinforcements will reduce the reinforcement orientation efficiency factor as in a 2D-random and 3D-random composite, respectively.

5.4 EFFECT OF OFF-AXIS LOADS ON PFRP TENSILE PROPERTIES

5.4.1 Off-axis loading of composites

Composites in load-bearing applications are often exposed to off-axis loads, which are loads at an angle to the primary fibre orientation (Fig. 5.1c). As mentioned in Section 5.1, the anisotropic nature of composites implies that off-axis loads have a significant detrimental effect on their effective mechanical properties. In fact, as the loading direction is varied from parallel to the principal fibre direction to normal to the principal fibre direction, the mechanical behaviour of the composite changes from fibre-dominated to matrix-dominated [57]. Testing the effect of off-axis loads is not only useful but also critical in understanding and assessing the manner in which

composite mechanical properties degrade as the loading direction is changed from the optimum fibre direction.

Although there are several researchers who have looked at longitudinal and transverse tensile properties of aligned PFRPs (for instance [7, 58]), there are limited articles that have evaluated tensile properties for a range of loading angles. Kumar [59] tested jute-polyester composites only in three directions – 0, 45 and 90°. Although Ntenga *et al.* [60] and Cichocki *et al.* [61] considered the effect of at least five off-axis angles other than 0 and 90°, to investigate the (thermo-)elastic anisotropy of aligned PFRPs they only measured elastic properties. Their studies focussed on the application of micro-mechanical models. The only complete results are by Madsen *et al.* [8] who measured tensile properties (modulus, strength and failure strain) of unidirectional hemp/PET in the directions 0, 10, 20, 30, 45, 60 and 90°. They found that the tensile modulus and strength drop drastically with increasing loading angle, as traditional composite laminate models predict. Nonetheless, more experimental data is required for further validation.

This section aims to *i*) characterise the stress-strain response, *ii*) investigate the tensile properties, and *iii*) analyse the fracture modes, of vacuum-infused unidirectional flax/polyester composites subjected to off-axis tensile loading. This study also looks to determine whether conventional composite micro-mechanical models can be used with confidence to quantitatively describe the off-axis tensile behaviour of PFRPs.

5.4.2 Experimental methodology

5.4.2.1 Reinforcement material

Flax yarn (Fig. 5.11) was obtained from Composites Evolution (UK). This is the same yarn (F50) used for the study in *Chapters 3 and 4*. The flax yarn (250 tex) employs a S-twist polyester filament binder (32 tex, ~13 wt% of yarn). This binder enables the core flax fibres to be of low twist (50 tpm, mean twist angle of 3.3°). The density of the flax yarn ρ_f (inclusive of the polyester binder) was measured, by

helium pycnometry, to be 1.529 ± 0.003 gcm⁻³. Formax (UK) Ltd produced 300 gsm stitched unidirectional (0°) and biaxial ($\pm 45^{\circ}$) fabrics from this yarn.

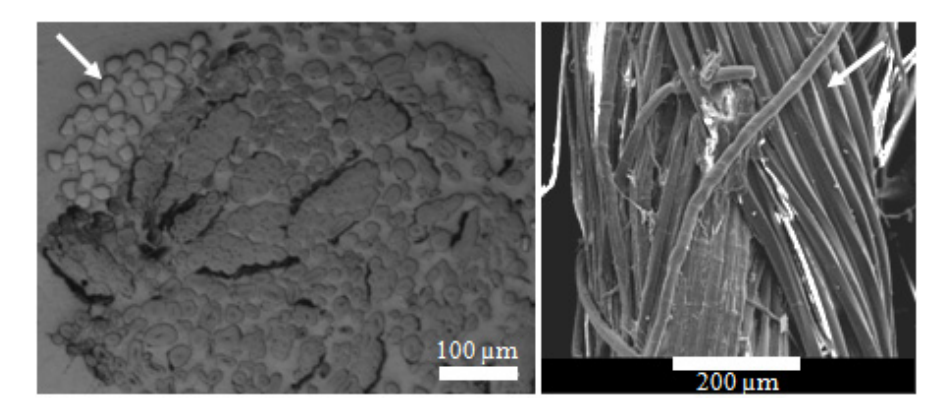


Fig. 5.11. Low twist flax yarn: optimal microscope image of cross-section (left) and SEM image of surface (right), showing the core flax fibres and polyester binder (indicated by arrow).

5.4.2.2 Composite manufacture

To study off-axis properties of the composites, the unidirectional fabric was laid-up in an aluminium mould tool at different inclination angles (0, 15, 30, 45, 60 and 90°). Unidirectional composite laminates (250 mm square, 3-3.5 mm thick) were manufactured from four layers of the as-received fabric using the vacuum infusion technique. Resin infusion was carried out at 70-80% vacuum (200-300 mbar absolute pressure).

An unsaturated polyester (Reichhold Norpol type 420-100) matrix was used. The resin was mixed with 0.25 wt% NL49P accelerator (Cobalt(II) 2-ethyl hexanoate, 1% Co in di-isobutyl phthalate) and 1 wt% Butanox M50 MEKP initiator. Post cure was carried out at 55 °C for 6 h after ambient cure for 16 h. From the manufacturer's datasheet, the polyester resin has a cured density ρ_m of 1.202 g·cm⁻³, tensile modulus E_m of 3.7 GPa, tensile strength σ_m of 70 MPa and failure strain ε_m of 3.5%. Taking the matrix Poisson's ratio v_m as 0.38 for cured polyester [52, 61, 62] and assuming isotropic properties, the matrix shear modulus G_m is estimated to be 1.34 GPa (Eq. 5.26).

$$G_m = \frac{E_m}{2(1 + \nu_m)}$$
 Eq. 5.26

Noting the mass of the fabric preform and the resulting composite plaque, the fibre weight fraction w_f of the laminates was determined. The composite density ρ_c was measured using helium pycnometry. The composite fibre volume fraction v_f was then determined using Eq. 5.27, allowing for porosity v_p .

$$v_f = \frac{\rho_c}{\rho_f} w_f; \quad v_m = \frac{\rho_c}{\rho_m} (1 - w_f); \quad v_p = 1 - (v_f + v_m)$$
 Eq. 5.27

The laminates have almost identical fibre volume fraction v_f of 26.9 ± 0.6 %, while the void content v_p ranges from 0.7–1.3%. Fig. 5.13 presents images of example test specimens; the off-axis angles are clearly visible from the sample surface. For comparative purposes, a laminate was also manufactured using the biaxial flax fabric ($v_f = 28.6$ %). Although ~13 wt% (~11 v%) of the flax yarn is polyester filament, it is assumed that flax fibre accounts for the total fibre volume fraction. The polyester filament has a density and tensile strength (~1.39 gcm⁻³, 539-1181 MPa) similar to flax fibre (1.40-1.55 gcm⁻³, 343-1035 MPa) [30].

5.4.2.3 Tensile testing

After the manufacture of composite laminates, tensile tests were conducted according to ISO 527-4:1997 (BS 2782-3:1997) [63] using an Instron 5985 testing machine equipped with a 100 kN load cell and an extensometer. Samples from the unidirectional laminates were loaded with the fibres at the defined inclination angles $(0, 15, 30, 45, 60 \text{ and } 90^{\circ})$ to the testing direction, while the biaxial samples were loaded in bias extension with fibres at $\pm 45^{\circ}$ to the testing direction. At least six 250 mm long and 25 mm wide specimens were tested for each type of composite at a cross-head speed of 2 mm/min. The elastic Young's modulus E_c , ultimate tensile strength σ_c , and failure strain ε_c were determined from the stress-strain data (Fig. 5.12). As Fig. 5.12b illustrates, the tensile modulus E_c is determined using the initial tangent modulus in the strain range of 0.025–0.100%. Note that the tensile modulus is not the same as the 'apparent stiffness'. Finally, the fracture surfaces of the failed

specimen were sputter coated with platinum and observed under a Philips XL30 SEM (acceleration voltage of 15 kV).

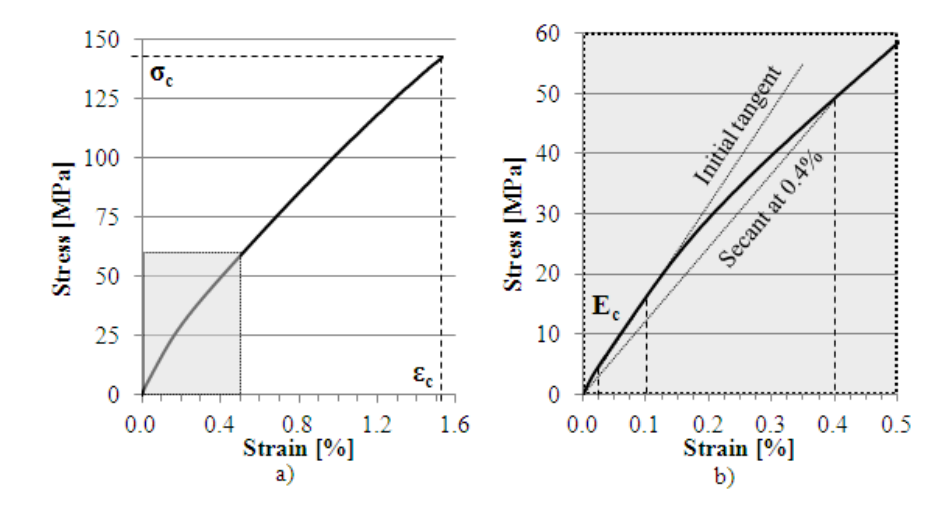


Fig. 5.12. Tensile mechanical properties extracted from the material stress-strain curve. The elastic Young's modulus E_c is determined using the initial tangent modulus in the strain range of 0.025-0.100%. The 'apparent stiffness' at ϵ % strain can be determined using the slope of the secant at ϵ % strain.

5.4.3 Results and Discussion

5.4.3.1 Tensile stress-strain behaviour

The typical stress-strain curves in Fig. 5.13 reveal the general changes in tensile properties of flax/polyester composites loaded at various off-axis angles. As the curves shift downwards for increasing loading angles, deterioration in composite tensile properties is observed. Essentially, the tensile modulus, strength and failure strain decrease with increasing misorientation.

As Fig. 5.13 illustrates, it is interesting that biaxial flax/polyester composites have a significantly higher failure strain of 3.76 ± 0.68 % compared to the other off-axis loaded unidirectional composites. With a tensile modulus and strength of 5.7 ± 0.1 GPa and 51.4 ± 2.8 MPa respectively, biaxial flax/polyester composites perform better than uniaxial flax/polyester composites loaded at 30° (Fig. 5.13). Thus, it can be said that biaxial composites are a better option than uniaxial composites for applications where loads are at an off-axis angle larger than 30°. Chamis [64]

concluded the same in their investigation of the off-axis tensile properties of unidirectional and bidirectional graphite-epoxy composites ($v_f \approx 50\%$).

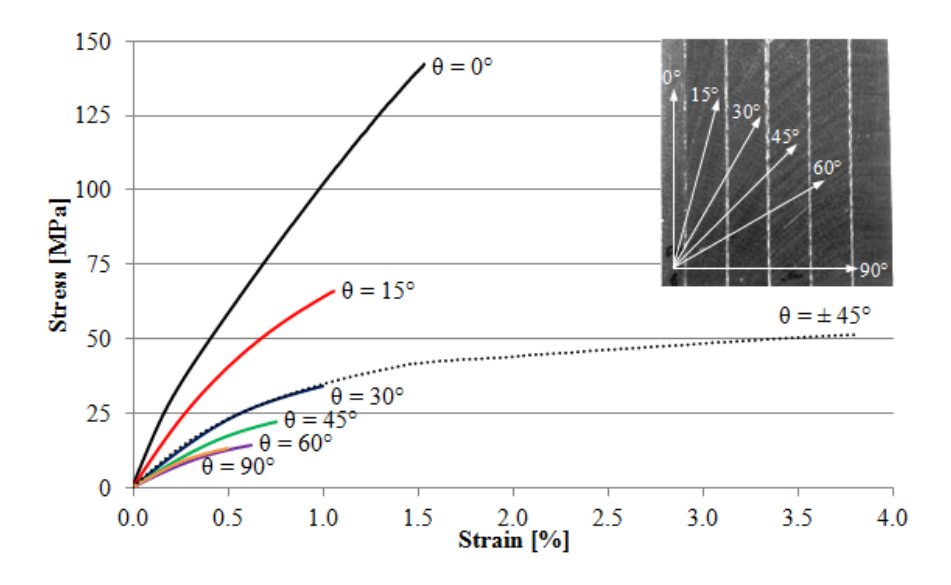


Fig. 5.13. Typical stress-strain curves of off-axis loaded unidirectional flax/polyester composites. Example test specimens are shown on the top right-hand corner. The typical stress-strain curve of a biaxial flax-polyester composite (loaded at $\pm 45^{\circ}$) is also shown.

Fig. 5.12 and Fig. 5.13 also show that even at low strains (< 0.5%) the stress-strain response of PFRPs, like single plant fibres [17, 23, 26, 65, 66], is non-linear. This is better observed in a plot of 'apparent stiffness' against strain (Fig. 5.14). Here, the apparent stiffness at ε % strain is defined as the secant modulus at ε % strain (shown in Fig. 5.12b).

The elastic Young's modulus is typically measured in the strain range of 0.05–0.25% (ISO 527-4:1997/BS 2782-3:1997 [63]). As Fig. 5.14 illustrates, while the apparent stiffness is fairly constant in this strain range for unidirectional E-glass–polyester composites due to their linear stress-strain curve ($v_f \approx 43\%$; material data from *Chapter 3*), there is significant variation in the apparent stiffness for PFRPs due to their non-linear stress-strain curve. In fact, the apparent stiffness of all the flax/polyester laminates reduces by ~30% in the strain range of 0.05–0.25%. Baets *et al.* [37] have also noticed this evolution in apparent stiffness for flax/epoxy composites. This observation has major implications on the strain range to be used

for the determination of the elastic Young's modulus. To overcome this issue, Baets et al. [37] measured the tensile modulus in the strain range of 0.05–0.10%. In this study (and in fact, all studies in this thesis), the tensile modulus is measured in the strain range of 0.025–0.100%. Both approaches are acceptable as ISO 527-4:1997 [63] recommends determining the secant modulus at 0.1% strain as the tensile modulus, if the tangent modulus in the strain range of 0.05–0.25% cannot be measured.

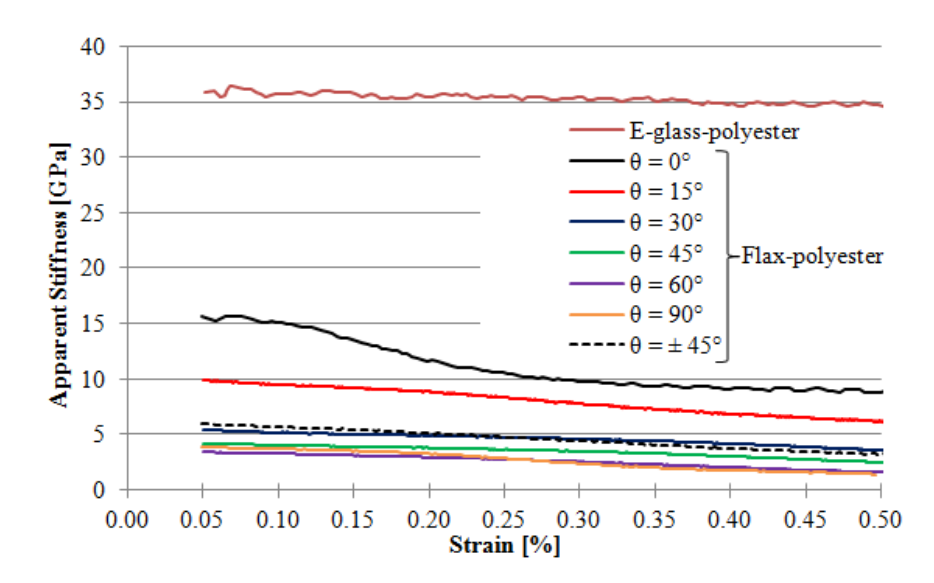


Fig. 5.14. Evolution of the apparent stiffness (secant modulus) with strain, for off-axis loaded flax/polyester composites. In the region of <0.25% strain, the apparent stiffness drops significantly for flax/polyester, but remains fairly constant for E-glass-polyester.

Cyclic stress-strain behaviour

The proposal to measure the elastic Young's modulus for PFRPs in the strain range of 0.025–0.100% becomes more attractive when the cyclic stress-strain behaviour of the material is studied. Elastic deformation is reversible and non-permanent; hence, there exists an elastic limit beyond which non-reversible permanent deformation occurs. To determine the elastic strain limit for PFRPs, six tensile specimens of unidirectional (0°) flax/polyester were subjected to successively larger loading-unloading cycles (load-unload rate of 7000 N/min). The applied load regime and the typical stress-strain response of the material are presented in Fig. 5.15a and b,

respectively. From the stress-strain response, the hysteresis and the effective plastic strain at the end of every cycle can be determined. The results are tabulated in Table 5.3.

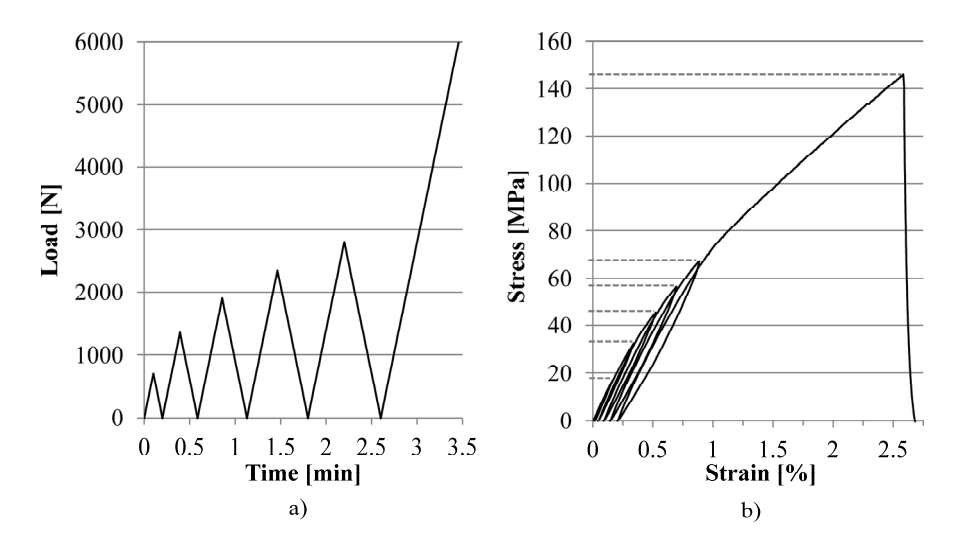


Fig. 5.15. *a)* Unidirectional (0°) flax/polyester composites were subjected to successively larger loading-unloading cycles with load increasing in every cycle. *b)* From the stress-strain response of the material, the plastic strain upon unloading after every cycle can be recorded.

Table 5.3. Strain upon loading and plastic strain upon unloading for unidirectional flax/polyester composites subjected to the load regime in Fig. 5.15a.

Cycle	Maximum Load [N]	Strain upon loading [%]	Plastic strain upon unloading [%]
1	700	0.165 ± 0.005	0.016 ± 0.002
2	1350	0.343 ± 0.011	0.046 ± 0.006
3	1900	0.528 ± 0.017	0.094 ± 0.010
4	2350	0.703 ± 0.026	0.146 ± 0.010
5	2800	0.895 ± 0.033	0.205 ± 0.006
6	Up to failure	2.476 ± 0.182	

If the material has been loaded in the elastic range, the plastic strain upon unloading will be zero. From the distinctive growing hysteresis loops in Fig. 5.15b and the analysed data in Table 5.3, it is seen that the plastic strain upon unloading increases

with applied load. Hence, there is certainly a degree of irreversibility in the deformation process of the microstructure. In addition, a non-zero plastic strain (of 0.016%) is observed even when the composite is loaded up to only 0.165% tensile strain. Using the results in Table 5.3, a linear regression analysis between strain upon loading and plastic strain upon unloading ($R^2 = 0.989$), suggests that the plastic strain is zero for tensile loading up to 0.146%. Consequently, the elastic Young's modulus for PFRPs can only be determined below this elastic strain limit of ~0.15%. Hughes *et al.* [67] conducted a similar study on flax/polyester composites and also found that this 'yield point' occurred at an average strain of 0.12%. In essence, measuring the tensile modulus for PFRPs in the strain range of 0.025–0.100% is sensible. Again, note that the composite tensile modulus has been measured in this strain range for all studies in this thesis.

Although the causes of the non-linear stress-strain response of the PFRPs (and the resulting stiffness reduction at low strains) are not yet clear [37, 67], they are possibly a result of 'non-reversible reorientation' on two length scales: *i*) untwisting/stretching of the reinforcing twisted staple fibre yarns [8, 37, 68], and *ii*) rigid body rotation and subsequent stretching and aligning of the cellulose microfibrils in a single plant fibre [12, 37, 65, 67]. The latter is believed to have a dominant role; particularly as plant single fibres themselves have a non-linear response to tensile loading (described in Section 5.2).

Several studies (for instance, [17, 23, 26, 28, 65, 66]) suggest that the non-linear stress-strain response of plant single fibres is a result of the initial misorientation of the cellulose microfibrils (represented by the MFA) and the 'non-reversible' uncoiling/aligning of the microfibrils upon loading. Burgert *et al.* [26] and Spatz *et al.* [28] have attempted to explain this phenomenon in more detail by comparing the tensile stress-strain response of low and high MFA single fibres. Spatz *et al.* [28] show that the yield point (or elastic limit) for single plant fibres, like PFRPs, is also very low. They argue that irreversible permanent plastic deformation above the yield point causes the non-linear stress-strain curve. They propose, with some critical backing from experimental evidence, that the irreversible visco-elasto-plastic deformation is driven by *i*) various complex micro-damage mechanisms, and *ii*)

structural changes (reorientation of microfibrils). Discussing the former, Burgert *et al.* [26] and Spatz *et al.* [28] suggest that the possible order of micro-damage progression is: *a)* the shear deformation and consequent viscous flow of the lignin-hemicellulose matrix, *b)* the sliding of cellulose microfibrils past each other, *c)* the consequential breakage and reformation of hydrogen bonds between fibril-fibril and fibril-matrix, and *d)* the continuous stripping of cellulose bridging hemicellulose chains. Hughes *et al.* [67] have also suggested that microstructural defects in the fibre (in the form of kink bands), may directly contribute to the non-linear strain behaviour of plant fibres and thus their composites. At least, the fact that the stress-strain response is linear for E-glass and its composites, and non-linear for plant fibres and their composites PFRPs, highlights *i)* the fundamental differences in the fibres, and *ii)* the varying stress-strain and damage accumulation mechanisms in the fibres and composites.

5.4.3.2 Theory and comparison with experiments

The tensile properties of a composite at a given off-axis loading angle can be estimated by well-known micro-mechanical models, such as the Tsai-Hill criterion [50]. These models are valid for transversely isotropic laminates under plane stress conditions. Unidirectional PFRPs are composed of transversely isotropic fibres/yarns embedded in an isotropic matrix, and hence they satisfy this requirement [8, 48, 60]. Here, comparisons are made between experimental data and predicted results from micro-mechanical models to i) show the validity of conventional composite models for PFRPs and ii) determine, otherwise difficult to measure, material properties (for instance, fibre shear modulus G_f and transverse tensile modulus $E_{f,90}$) through numerical methods. Note that in this study, the contribution of yarn twist to effective ply orientation θ has been neglected, as low-twist flax yarns have been used.

Elastic properties

The influence of ply orientation θ on the tensile modulus E_c of the composites is graphically presented in Fig. 5.16. Unidirectional flax/polyester composites loaded in the fibre direction (0°) have a stiffness $E_{c,\theta}$ of 15.3 \pm 0.6 GPa. This is 4 times higher than the composite transverse tensile modulus $E_{c,\theta\theta}$ of 3.8 \pm 0.2 GPa. Madsen *et al.*

[8] noted a similar anisotropy ratio between longitudinal (17.6 \pm 0.7 GPa) and transverse tensile modulus (3.5 \pm 0.1 GPa) from tests on hemp/PET composites ($v_f \approx$ 33.5%).

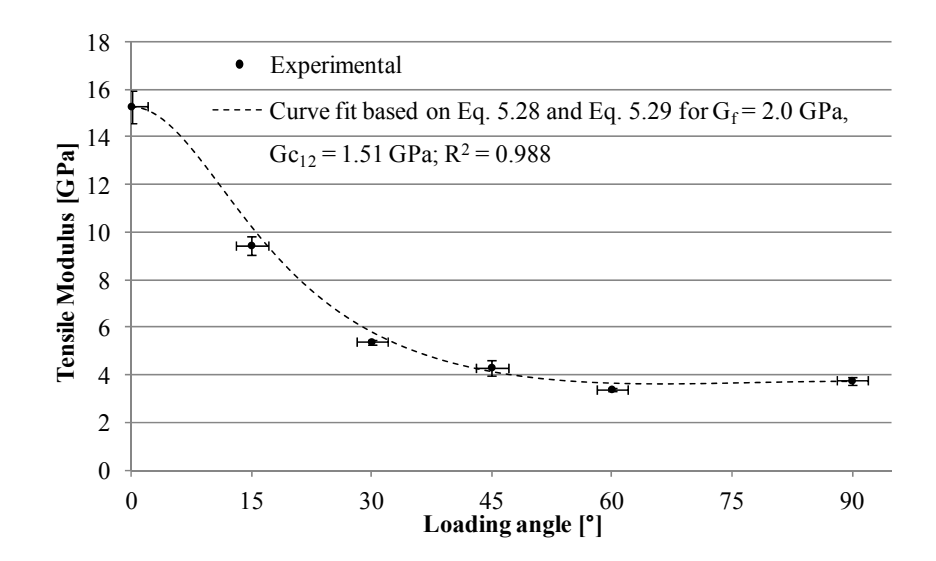


Fig. 5.16. Variation in tensile modulus of unidirectional flax/polyester composites for increasing off-axis loading angle. Experimental data (•) is presented with error bars (1 stdev). The dotted line is a theoretical prediction based on Eq. 5.28 and Eq. 5.29 for $G_f = 2.0$ GPa (and $G_{c12} = 1.51$ GPa).

It is observed from Fig. 5.16 that the composite tensile modulus drops significantly for increasing loading angle between $0^{\circ} < \theta < 30^{\circ}$. While it is of interest to note that composites loaded at $\theta = 60^{\circ}$ have the lowest tensile modulus, there is little variation in composite stiffness for $30^{\circ} < \theta < 90^{\circ}$. Assuming that the unidirectional laminates are transverse isotropic structures under plane stress conditions, Eq. 5.28 can be used to predict the change in composite tensile modulus for increasing off-axis loading angle, given that four composite properties are known: longitudinal and transverse tensile modulus ($E_{c,0}$, $E_{c,90}$), shear modulus G_{c12} and Poisson's ratio V_{c12} .

$$E_{c,\theta} = \left[\frac{1}{E_{c,0}} \cos^4 \theta + \left(\frac{1}{G_{c12}} - \frac{2\nu_{c12}}{E_{c,0}} \right) \cos^2 \theta \sin^2 \theta + \frac{1}{E_{c,90}} \sin^4 \theta \right]^{-1}$$
 Eq. 5.28

The composite longitudinal and transverse stiffness $(E_{c,0}, E_{c,90})$ have been experimentally determined. The Poisson's ratio v_{c12} of the composite is taken to be

0.31 [61]. The composite shear modulus G_{c12} can be estimated using the semiempirical Halpin-Tsai equation [69] (Eq. 5.29). The Halpin-Tsai equation expresses the composite shear modulus G_{c12} as a function of the fibre shear modulus G_f . Hence, the fibre shear modulus G_f can be adjusted to determine a composite shear modulus G_{c12} (using Eq. 5.29) that best fits the experimental data. Here, best fit is determined using least squares (non-linear) regression \mathbb{R}^2 values.

$$G_{c12} = \frac{G_m (1 + \xi \eta v_f)}{(1 - \eta v_f)}, \text{ where } \eta = \frac{\frac{G_f}{G_m} - 1}{\frac{G_f}{G_m} + \xi}$$
 Eq. 5.29

In Eq. 5.29, a fibre shape factor ξ needs to be entered. ξ correlates to the geometry (aspect ratio) of the reinforcement, but also packing arrangement and loading conditions [70]. Typically, assuming circular cross-section fibres [69, 70] and using ξ = 1 produces satisfactory results for PFRPs [8, 17]. However, it is well known that the cross-section of plant fibres is variable, irregular and non-circular. Only recently have researchers quantitatively estimated the deviation of the fibre cross-section shape from circularity [71-73]. The studies suggest that calculating the cross-section area A_C, assuming a circular cross-section with an average fibre diameter 'd', overestimates the true cross-section area A_T by a factor κ of 1.42–2.55 [71-73]. Therefore, in this study, an attempt is made to use a value of ξ representative of the non-circular cross-section of plant fibres. Some studies, for instance [18, 74], show that an ellipse is a much better model of a natural fibre cross section than a circle. If the true fibre cross-section A_T is assumed to be elliptical with major axis 'a' and minor axis 'b', the factor κ is equal to the ratio a/b (shown in Eq. 5.30). As ξ depends on cross-sectional aspect ratio [70], assuming an elliptical fibre cross-section should suffice in estimating the resulting anisotropy. Halpin and Kardos [70] have semiempirically derived Eq. 5.31 to determine the fibre shape factor ξ for composites with elliptical/rectangular cross-section fibres to calculate G_{c12} . As a quick check of Eq. 5.31, in the limiting case for circular cross-section fibres, $\xi = 1$ since a = b. For elliptical cross-section plant fibres with a/b = 1.42-2.55, $\xi = 1.84-5.06$ should be

used to determine G_{c12} . The effect of ξ on G_{c12} is found to be negligible; for $G_f = 2.0$ GPa, G_{c12} ranges from 1.49–1.51 for ξ ranging from 1.00–5.06.

$$\kappa = \frac{A_C}{A_T} = \frac{\pi \frac{d^2}{4}}{\pi \frac{ab}{4}} = \frac{d^2}{ab} = \frac{a}{b} \quad \text{(for } \kappa > 1 \text{ and assuming } d = a\text{)}$$
 Eq. 5.30

$$\xi = \left(\frac{a}{b}\right)^{\sqrt{3}} \quad \text{(for } G_{c12}\text{)}$$
 Eq. 5.31

Fig. 5.16 shows that using $G_{c12} = 1.51$ GPa (taking $G_f = 2.0$ GPa in Eq. 5.29) gives the best fit Eq. 5.28 for the experimental data of flax/polyester. Using the shear modulus of native cellulose as 4.4 GPa [18], Baley [17] estimated the shear modulus of flax fibre to be in the range of $G_f = 2.4$ –3.4 GPa. For jute/epoxy composites, Cichocki *et al.* [61] measured G_f and G_{c12} to be 3.5 GPa and 1.4 GPa, respectively. In a study by Ntenga *et al.* [60] G_{c12} was measured to be 1.68–2.04 GPa for sisal–epoxy composites. Hence, the shear modulus of flax and its composite determined in this study are in agreement with other studies in literature.

The macroscopic response of the composite, in the form of longitudinal and transverse stiffness, can be incorporated in other micro-mechanics equations to determine fibre properties. The longitudinal tensile modulus $E_{f,\theta}$ of the flax fibres can be back-calculated using the rule of mixtures (Eq. 5.32) to be $E_{f,\theta} = 46.3$ GPa. This is in the range of literature values [13, 30] generally quoted for flax.

$$E_{f,0} = \frac{1}{v_f} \left[E_{c,0} - v_m E_m \right]$$
 Eq. 5.32

The transverse tensile modulus $E_{f,90}$ of the flax fibres can be estimated by rearranging the semi-empirical Halpin-Tsai equation [69] from Eq. 5.33 to Eq. 5.34. Typically, assuming circular cross-section flax fibres [69, 70] and using $\xi = 2$ produces satisfactory results for PFRPs [8, 17]. Halpin and Kardos [70] have semi-empirically derived Eq. 5.35 to determine the fibre shape factor ξ for composites with elliptical/rectangular cross-section fibres to calculate $E_{f,90}$. As a quick check of Eq. 5.35, in the limiting case for circular cross-section fibres, $\xi = 2$ since a = b. For

elliptical plant fibres with a/b = 1.42-2.55, $\xi = 2.84-5.10$ should be used to determine $E_{f,90}$. Again, it should be noted that the effect of ξ on $E_{f,90}$ is found to be negligible. Substituting the relevant material data (E_m , $E_{c,90}$, v_f) into Eq. 5.34 gives the transverse tensile modulus of flax to be $E_{f,90} = 3.9$ GPa for $\xi = 2.84-5.10$. Nonetheless, this estimate of fibre transverse tensile modulus $E_{f,90}$ is in the range of values found by other researchers: 5–9 GPa for flax fibres [58], 5.5 GPa for jute fibres [61] and 1.4 GPa for sisal fibres [60]. The ratio of longitudinal to transverse fibre stiffness is 11.7 and hence the fibres are highly anisotropic. This is also in agreement with findings from other studies, where fibre anisotropy ratios of 8.4 for flax [58], 7.2 for jute [61], 7.7 for hemp [8] and 8.1 for sisal [60] have been reported.

$$E_{c,90} = \frac{E_m (1 + \xi \eta v_f)}{(1 - \eta v_f)}, \text{ where } \eta = \frac{\frac{E_{f,90}}{E_m} - 1}{\frac{E_{f,90}}{E_m} + \xi}$$
 Eq. 5.33

$$E_{f,90} = \frac{E_m \xi (1 - v_f) - E_{c,90} (\xi + v_f)}{\frac{E_{c,90}}{E_m} (1 - v_f) - (1 + \xi v_f)}$$
 Eq. 5.34

$$\xi = 2\left(\frac{a}{b}\right) \text{ (for } E_{c,90}\text{)}$$
 Eq. 5.35

Fracture stress

The influence of ply orientation θ on the tensile strength σ_c of the composites is graphically presented in Fig. 5.17. Unidirectional flax/polyester composites loaded in the fibre direction (i.e. 0°) have a tensile strength σ_0 of 143.0 ± 6.8 MPa. This is 10.8 times higher than the composite transverse tensile strength σ_{90} of 13.2 ± 0.4 MPa. Madsen *et al.* [8] noted a similar ratio between longitudinal (205 ± 5 GPa) and transverse tensile strength (19 ± 0 GPa) from tests on hemp/PET composites ($v_f \approx 33.5\%$).

Again, it is observed from Fig. 5.17 that the composite tensile strength drops significantly for increasing loading angle between $0^{\circ} < \theta < 30^{\circ}$. For $30^{\circ} < \theta < 90^{\circ}$, there is little variation in composite strength. The composite off-axis fracture stress

 σ_{θ} can be predicted using either the maximum stress (Stowell-Liu) criterion [52] or the maximum strain energy (Tsai-Hill) criterion [50]. The maximum stress criterion is defined by three equations (Eq. 5.36), each of which characterises three failure regimes. The Tsai-Hill criterion is defined by Eq. 5.37. Both failure criteria require three known composite properties: longitudinal and transverse tensile strength (σ_{θ} , σ_{θ}) and inter-laminar shear strength τ . As σ_{θ} and σ_{θ} 0 have been measured, it is possible to adjust the value of τ , so that the micro-mechanical criteria can be used to fit the experimental data using least squares non-linear regression.

$$\sigma_{\theta} = \begin{cases} \frac{\sigma_{0}}{\cos^{2}\theta} & \text{(longitudnal tensile failure of fibres, } \theta < 5^{\circ} \text{)} \\ \frac{\tau}{\sin\theta\cos\theta} & \text{(shear failure at fibre/matrix interface, } 5^{\circ} < \theta < 45^{\circ} \text{)} \end{cases}$$
 Eq. 5.36
$$\frac{\sigma_{90}}{\sin^{2}\theta} & \text{(transverse tensile failure of fibres, } 45^{\circ} < \theta < 90^{\circ} \text{)}$$

$$\sigma_{\theta} = \left[\frac{1}{\sigma_0^2} \cos^4 \theta + \left(\frac{1}{\tau^2} - \frac{1}{\sigma_0^2} \right) \cos^2 \theta \sin^2 \theta + \frac{1}{\sigma_{90}^2} \sin^4 \theta \right]^{-0.5}$$
 Eq. 5.37

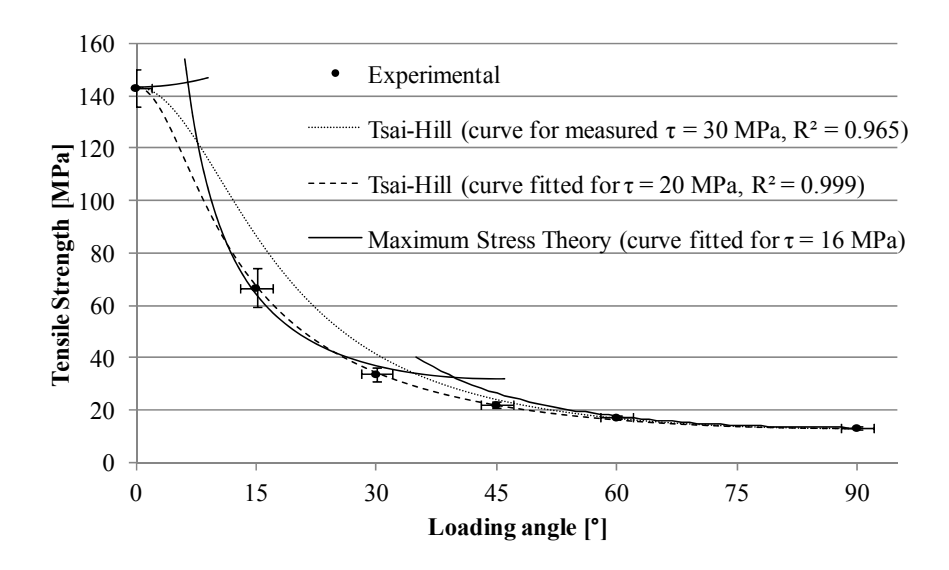


Fig. 5.17. Variation in tensile strength of unidirectional flax/polyester composites for increasing off-axis loading angle. Experimental data (\bullet) is presented with error bars (1 stdev). Lines are theoretical predictions using Tsai-Hill criterion (dotted) and maximum stress theory (solid) for different composite shear strength τ .

From Fig. 5.17, it is observed that the maximum stress criterion and the Tsai-Hill criterion are in good agreement with the experimental data, for $\tau = 16$ MPa and 20 MPa, respectively. Chamis and Sinclair [75, 76] have reported that the inter-laminar shear strength can be extracted from the 10° off-axis tensile test of a unidirectional specimen. Although the tensile strength of a unidirectional flax/polyester specimen loaded at an off-axis angle of 10° has not been tested in this study, data from the 15° off-axis test can be used to estimate the inter-laminar shear strength to be $\tau = 16.7$ MPa. This is in good agreement with the estimated inter-laminar shear strength of 16-20 MPa (Fig. 5.17).

Incorporating the effect of yarn twist

Curve fitting methods and micro-mechanical criteria (Eq. 5.28, Eq. 5.36 and Eq. 5.37) have enabled accurate prediction of the dependence of PFRP tensile properties (stiffness and strength) on ply orientation. As an extension, it is possible to rearrange Eq. 5.28 and Eq. 5.37 in the form of Eq. 5.38 and Eq. 5.39 respectively. This is useful for two reasons. Firstly, Eq. 5.38 and Eq. 5.39 require stiffness ratios $(E_{c,0}/G_{c12}, E_{c,0}/E_{c,90})$ and strength ratios $(\sigma_0/\sigma_{90}, \sigma_0/\tau)$ as inputs. Typical values of these ratios are presented in Table 5.4. These values can be used in conjunction with Eq. 5.38 and Eq. 5.39 for preliminary design of structural composites from PFRPs.

$$\frac{E_{c,\theta}}{E_{c,0}} = \left[\cos^4\theta + \left(\frac{E_{c,0}}{G_{c12}} - 2\nu_{c12}\right)\cos^2\theta\sin^2\theta + \frac{E_{c,0}}{E_{c,90}}\sin^4\theta\right]^{-1}$$
 Eq. 5.38

$$\frac{\sigma_{\theta}}{\sigma_{0}} = \left[\cos^{4}\theta + \left(\left(\frac{\sigma_{0}}{\tau}\right)^{2} - 1\right)\cos^{2}\theta\sin^{2}\theta + \left(\frac{\sigma_{0}}{\sigma_{90}}\right)^{2}\sin^{4}\theta\right]^{-0.5}$$
 Eq. 5.39

Secondly, while the contribution of yarn twist on ply orientation has been neglected in this study, Eq. 5.38 and Eq. 5.39 can be modified to accommodate for the effect of yarn twist on the off-axis tensile properties of PFRPs. In Section 5.3, we developed a mathematical model that accurately predicts the effect of reinforcing yarn surface twist angle α on PFRP tensile strength σ_0 . Baets *et al.* [37] have also applied existing models which relate yarn surface twist angle α to PFRP tensile modulus $E_{c,0}$. These models can be substituted for $E_{c,0}$ and σ_0 in Eq. 5.38 and Eq. 5.39.

Table 5.4. Typical values of strength and stiffness ratios for unidirectional PFRPs found from literature.

	v_f	$E_{c,0}$			σ_0				
Composite	[%]	[GPa]	$E_{c,0}/E_{c,90}$	$E_{c,0}/G_{c12}$	[MPa]	σ_0/σ_{90}	σ_0/ au	v_{c12}	Source
Flax/polyester	26.9	15.3	4.1	10.1	143	10.8	7.2	-	
Hemp/PET	33.5	17.6	5.0	9.3	205	10.8	7.9	-	[8]
Jute/epoxy	30.0	13.8	3.7	9.9	-	-	-	0.31	[61]
Flax/epoxy	40.0	26.0	6.5	-	190	19.0	-	-	[7]
Flax/epoxy	48.0	32.0	8.0	-	268	14.9	-	-	[7]
Sisal/epoxy	39.0	6.9	2.6	3.7	-	-	-	0.42	[60]

While the resulting equations can then be used to obtain indicative off-axis properties inclusive of the contribution from yarn twist, the equations should be used with caution. This is because, unlike 2D ply orientation, yarn twist is a complex 3D phenomenon. Firstly, the twist angle of an arbitrary fibre in the yarn is a function of i) its radial position in the yarn, ii) yarn twist level, iii) yarn packing fraction and iv) yarn density. Secondly, the twist level of the reinforcing yarn will not only affect $E_{c,0}$ and σ_0 , but will also affect the stiffness and strength ratios, which are additional inputs to Eq. 5.38 and Eq. 5.39. In fact, the effect of yarn twist on i) in-plane ($E_{c,90}$, σ_{90} , G_{c12} , τ), ii) out-of-plane and iii) off-axis properties of PFRPs warrants specific investigation.

5.4.3.3 Fracture strain and fracture modes

The failure strain of unidirectional flax/polyester composites decreases with increasing off-axis loading angle (Fig. 5.18). While composites loaded in the fibre direction (*i.e.* 0°) have a failure strain of 1.56 ± 0.04 %, composites loaded in the transverse direction (*i.e.* 90°) have a failure strain of only 0.49 ± 0.03 %.

A more insightful observation is that while the transverse failure strain of unidirectional flax/polyester decreases linearly with increasing fibre content [58], the longitudinal failure strain of unidirectional flax/polyester increases with increasing fibre content, before levelling off. This is graphically presented in Fig. 5.19.

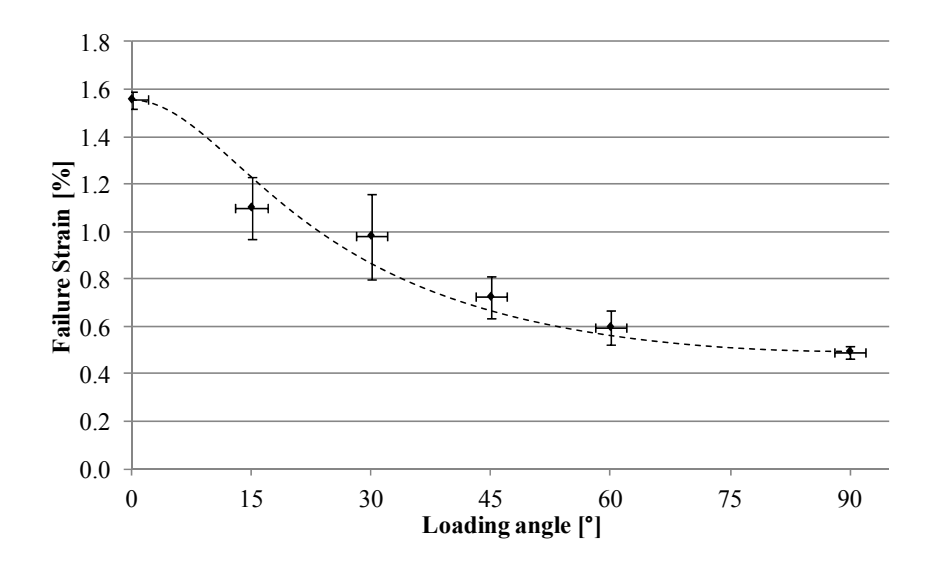


Fig. 5.18. Variation in failure strain of unidirectional flax/polyester composites for increasing off-axis loading angle.

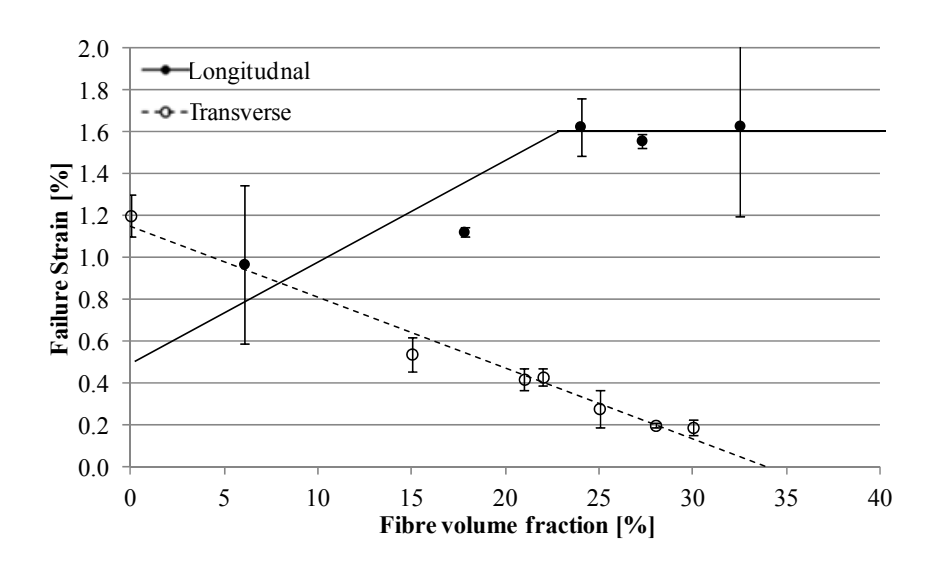


Fig. 5.19. Variation in (•) longitudinal and (o) transverse failure strain of unidirectional flax/polyester composites for increasing fibre volume fraction. Results are from *Chapter 4* (for longitudinal) and [58] (for transverse).

These observations are indicative of changes in failure mode with increasing off-axis loading angle. For low off-axis angles ($\theta < 5^{\circ}$), the composite failure strain of 1.56% is close to the tensile failure strain of a single flax fibre. The SEM micrograph in Fig. 5.20a) confirms that the composite fracture surface is serrated and irregular due to

Chapter 5

fibre-dominated failure. Extensive fibre pull-out is also observed and the lateral surfaces of these pulled out fibres are clear from matrix residue; this is indicative of poor adhesion between fibre and matrix. While some matrix laceration is observed, matrix cleavage and irregular fibre fracture surfaces are attributable to longitudinal tensile fracture of the composite [76]. As the fibres are failing in pure tension, the corollary is that increasing the fibre content would lead to an increase in the longitudinal failure strain of the composite, before levelling off at the fibre failure strain. This is observed in Fig. 5.19.

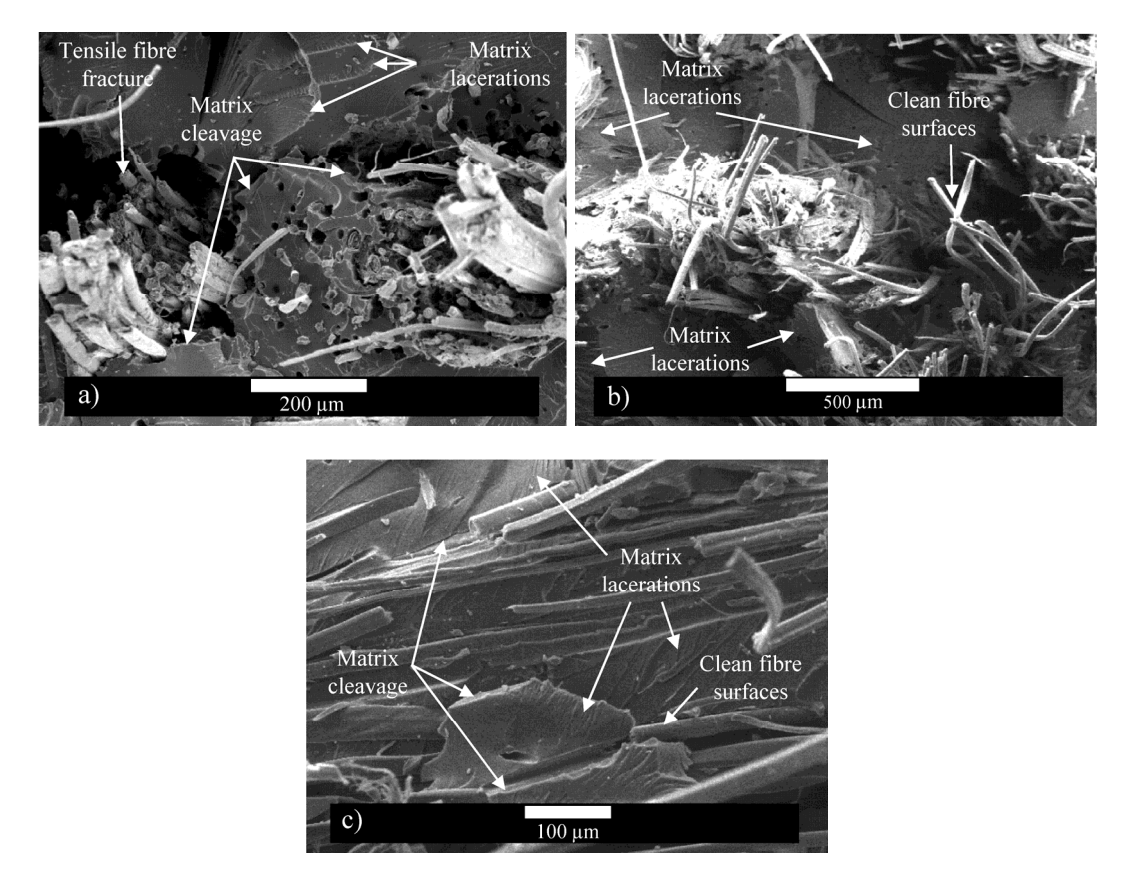


Fig. 5.20. Fracture surfaces of flax/polyester at different off-axis load angles present different fracture modes: a) $\theta = 0^{\circ}$, longitudinal tensile fracture, fibredominated failure; b) $\theta = 15^{\circ}$, inter-laminar shear; c) $\theta = 90^{\circ}$, transverse fracture, matrix-dominated failure.

In the range of $5^{\circ} < \theta < 45^{\circ}$, the fracture strain reduces drastically from 1.5% to 0.5%. As misorientation increases, inter-laminar shear stresses and then transverse tensile stresses become more dominant [75]. The SEM micrograph in Fig. 5.20b)

shows that the fracture surface is dominated by matrix lacerations, indicating some inter-laminar shear stress fracture [76]. Some matrix cleavage (with irregular boundary) is also observed due to transverse tensile fracture of the matrix [76]. Again the fibre surfaces are free from matrix residue due to poor interfacial bonding.

For off-axis angles in the range of $45^{\circ} < \theta < 90^{\circ}$, the failure strain is very low (0.5–0.7%). This is because flax fibres and their composites are highly anisotropic and transverse tensile stress is the predominant fracture mode in this range [75]. The SEM micrograph in Fig. 5.20c) confirms that the fracture surface is dominated by extensive matrix cleavage. However, some matrix laceration is observed in resin rich zones, indicating shear fracture. Baley *et al.* [58] have reported that during transverse failure of unidirectional flax/polyester composites, cracks propagate along the fibre-matrix interface. These observations are consistent with the fracture surface in Fig. 5.20c), as the fibre surfaces are free from matrix residue suggesting poor fibre-matrix adhesion. An increase in the fibre content would lead to more fibre-matrix interfaces. Hence, crack propagation would be easier and the failure strain would be smaller for high fibre content PFRPs loaded in the transverse direction [58]. This is observed in Fig. 5.19.

5.4.4 Conclusions

The highly anisotropic nature of plant fibres and their aligned composites implies that misorientation influences their tensile behaviour significantly. For PFRPs to be readily considered for structural applications, an experimental assessment of their off-axis mechanical behaviour is essential.

A key finding of this study is that due to the non-linear stress-strain response of PFRPs, the apparent stiffness of the composite reduces by $\sim 30\%$ in the strain range of 0.05–0.25%. In addition, through cyclic tests on the composites, the elastic strain limit is found to be only $\sim 0.15\%$. This has major implications on the strain range to be used for the determination of the composite elastic Young's modulus. Consequently, it is proposed that the tensile modulus for PFRPs should be measured in the strain range of 0.025–0.100%. It is argued that the non-linear stress-strain

response (decreasing 'apparent' stiffness with increasing strain) of single plant fibres has been transferred to the PFRPs.

The PFRP elastic modulus, tensile strength and failure strain reduce drastically with increasing off-axis loading angle. In fact, biaxial (±45°) composites have better mechanical properties than uniaxial composites loaded at off-axes angles larger than 30°. Conventional composite micro-mechanical models are found to be in good agreement with the experimental data, suggesting that reliable prediction of PFRP off-axis properties is possible. The application of such models has enabled the determination of, otherwise difficult to measure, material properties through numerical methods. For instance, the shear modulus and transverse modulus of flax fibre is determined to be 2.0 GPa and 3.9 GPa, respectively. Through qualitative analysis of the fracture surfaces of off-axis loaded PFRPs, three distinct fracture modes are determined in three different off-axis ranges.

5.5 REFERENCES

- 1. Carus M. Bio-composites: Technologies, applications and markets, in 4th International Conference on Sustainable Materials, Polymers and Composites. 6-7 July 2011. Birmingham, UK.
- 2. Faruk O, Bledzki AK, Fink HP, Sain M. Biocomposites reinforced with natural fibres: 2000-2010. *Progress in Polymer Science*, 2012, 37(11): p. 1552-1596.
- 3. Krenchel H. Fibre reinforcement. *Akademisk Forlag*, 1964: p. 16-22.
- 4. Lu Y. Mechanical properties of random discontinuous fiber composites manufactured from wet-lay process. MSc, 2002. Virginia Polytechnic Institute and State University: Blacksburg, Virginia.
- 5. Madsen B. *Properties of plant fibre yarn polymer composites An experimental study.* PhD, 2004. Technical University of Denmark: Lyngby, Denmark.
- 6. George J, Ivens J, Verpoest I. Mechanical properties of flax fibre reinforced epoxy composites. *Die Angewandte Makromolekulare Chemie*, 1999, 272(1): p. 41-45.
- 7. Weyenberg I, Chitruong T, Vangrimde B, Verpoest I. Improving the properties of UD flax fibre reinforced composites by applying an alkaline fibre treatment. *Composites Part A: Applied Science and Manufacturing*, 2006, 37: p. 1368-1376.
- 8. Madsen B, Hoffmeyer P, Lilholt H. Hemp yarn reinforced composites II. Tensile properties. *Composites Part A: Applied Science and Manufacturing*, 2007, 38: p. 2204-2215.
- 9. Mutje P, Girones J, Lopez A, Llop MF, Vilaseca F. Hemp strands: PP composites by injection molding: Effect of low cost physico-chemical treatments. *Journal of Reinforced Plastics and Composites*, 2006, 25: p. 313-327.
- 10. Shahzad A. Hemp fiber and its composites A review. *Journal of Composite Materials*, 2012, 46(8): p. 973-986.
- 11. Summerscales J, Hall W, Virk AS. A fibre diameter distribution factor (FDDF) for natural fibre composites. *Journal of Materials Science*, 2011, 46(17): p. 5876-5880.

- 12. Placet V, Trivaudey F, Cisse O, Gucheret-Retel V, Boubakar ML. Diameter dependence of the apparent tensile modulus of hemp fibres: A morphological, structural or ultrastructural effect? *Composites Part A: Applied Science and Manufacturing*, 2012, 43(2): p. 275-287.
- 13. Pickering K, ed. *Properties and performance of natural-fibre composites.* 2008. CRC Press LLC: Boca Raton.
- 14. Diddens I, Murphy B, Krisch M, Muller M. Anisotropic elastic properties of cellulose measured using inelastic x-ray scattering. *Macromolecules*, 2008, 41(24): p. 9755–9759.
- 15. Mark R. Cell wall mechanics of tracheids, 1967. New Haven: Yale University Press.
- 16. Nishino T, Takano K, Nakamae K. Elastic modulus of the crystalline regions of cellulose polymorphs. *Journal of Polymer Science B*, 1995, 33: p. 1647-1651.
- 17. Baley C. Analysis of the flax fibres tensile behaviour and analysis of the tensile stiffness increase. *Composites Part A: Applied Science and Manufacturing*, 2002, 33: p. 939-948.
- 18. Gassan J, Chate A, Bledzki AK. Calculation of elastic properties of natural fibers. *Journal of Materials Science*, 2001, 36: p. 3715-3720.
- 19. Bergander A, Salmen L. Cell wall properties and their effects on the mechanical properties of fibers. *Journal of Materials Science*, 2002, 37: p. 151-156.
- 20. Bledzki A, Gassan J. Composites reinforced with cellulose based fibres. *Progress in Polymer Science*, 1999, 24: p. 221-274.
- 21. McLaughlin E, Tait RA. Fracture mechanism of plant fibres. *Journal of Materials Science*, 1980, 15: p. 89-95.
- 22. Mukherjee P, Satyanarayana KG. An empirical evaluation of structure-property relationships in natural fibres and their fracture behaviour. *Journal of Materials Science*, 1986, 21: p. 4162-4168.
- 23. Reiterer A, Lichtenegger H, Tschegg S, Fratzl P. Experimental evidence for a mechanical function of the cellulose microfibril angle in wood cell walls. *Philosophical Magazine A*, 1999, 79(9): p. 2173-2184.
- 24. Sheng-zuo F, Wen-zhong Y, Xiang-xiang FU. Variation of microfibril angle and its correlation to wood properties in poplars. *Journal of Forestry Research*, 2004, 15(4): p. 261-267.
- 25. Via B, So CL, Shupe TF, Groom LH, Wikaira J. Mechanical response of longleaf pine to variation in microfibril angle, chemistry associated wavelengths, density, and radial position. *Composites Part A: Applied Science and Manufacturing*, 2009, 40: p. 60-66.
- 26. Burgert I, Fratzl P. Plants control the properties and actuation of their organs through the orientation of cellulose fibrils in their cell walls. *Integrative and Comparative Biology*, 2009, 49(1): p. 69-79.
- 27. Satyanarayana K, Pillai CKS, Sukumaran K, Pillai SGK, Rohatgi PK, Vijayan K. Structure property studies of fibres from various parts of the coconut tree. *Journal of Materials Science*, 1982, 17: p. 2453-2462.
- 28. Spatz H, Kohler L, Niklas KJ. Mechanical behaviour of plant tissues: composite materials or structures? *The Journal of Experimental Biology*, 1999, 202: p. 3269–3272.
- 29. Suslov D, Verbelen JP. Cellulose orientation determines mechanical anisotropy in onion epidermis cell walls. *Journal of Experimental Botany*, 2006, 57(10): p. 2183-2192.
- 30. Lewin M. *Handbook of fiber chemistry*. Third ed, 2007. Boca Raton: CRC Press LLC.

- 31. Barnett J, Bonham VA. Cellulose microfibril angle in the cell wall of wood fibres. *Biological Reviews*, 2004, 79: p. 461-472.
- 32. Dissanayake N, Summerscales J, Grove SM, Singh MM. Life cycle impact assessment of flax fibre for the reinforcement of composites. *Journal of Biobased Materials and Bioenergy*, 2009, 3(3): p. 1-4.
- 33. Finn N, Miao M. Low cost composite preforms from natural fibres, in *Composites Australia 2008: Conference & Exhibition*. 13-14 March 2008. Melbourne, Australia.
- 34. Arnold E, Weager, BM, Hoydonckx HE, Madsen B. Next generation sustainable composites: Development and processing of furan-flax biocomposites, in *17th International Conference on Composite Materials*. 27-31 July 2009. Edinburgh, UK.
- 35. Goutianos S, Peijs T, Nystrom B, Skrifvars M. Development of flax fibre based textile reinforcements for composite applications. *Applied Composite Materials*, 2006, 13(4): p. 199-215.
- 36. Goutianos S, Peijs T. The optimisation of flax fibre yarns for the development of high-performance natural fibre composites. *Advanced Composites Letters*, 2003, 12(6): p. 237-241.
- 37. Baets J, Plastria D, Ivens J, Verpoest I. Determination of the optimal flax fibre preparation for use in UD-epoxy composites, in *4th International Conference on Sustainable Materials, Polymers and Composites*. 6-7 July 2011. Birmingham, UK.
- 38. Zhang L, Miao M. Commingled natural fibre/polypropylene wrap spun yarns for structured thermoplastic composites. *Composites Science and Technology*, 2010, 70: p. 130-135.
- 39. Ma H, Li Y, Luo Y. The effect of fiber twist on the mechanical properties natural fiber reinforced composites, in *18th International Conference on Composite Materials*. 2011. Jeju, South Korea.
- 40. Rao Y, Farris, RJ. A modeling and experimental study of the influence of twist on the mechanical properties of high-performance fiber yarns. *Journal of Applied Polymer Science*, 2000, 77: p. 1938-1949.
- 41. Naik N, Madhavan V. Twisted impregnated yarns: Elastic properties. *Journal of Strain Analysis*, 2000, 35(2): p. 83-91.
- 42. Shioya M, Itoh T, Kunugi T, Takaku A. Variation of longitudinal modulus with twist for yarns composed of high modulus fibers. *Textile Research Journal*, 2001, 71: p. 928-936.
- 43. Baets J, Plastria D, Ivens J, Verpoest I. Determination of the optimal flax fibre preparation for use in UD-epoxy composites, in *18th International Conference on Composite Materials (ICCM-18)*. 2011. Jeju, South Korea.
- 44. Rask M, Madsen B. Twisting of fibres in yarns for natural fibre composites, in *18th International Conference on Composite Materials (ICCM-18)*. 2011. Jeju, South Korea.
- 45. Gegauff G. Force et elasticite des files en cotton. *Bulletin De La Societe Industrielle De Mulhouse*, 1907, 77: p. 153.
- 46. Platt M. Mechanics of elastic performance of textile materials, Part III: Some aspects of stress analysis of textile structures Continuous filament yarns. *Textile Research Journal*, 1950, 20: p. 1.
- 47. Hearle J, Grosberg P, Backer S. Structural mechanics of yarns and fabrics. Vol. 1 p. 180, 1969. New York: Wiley-Interscience.
- 48. Pan N. Development of a constitutive theory for short fiber yarns: Mechanics of staple yarn without slippage effect. *Textile Research Journal*, 1992, 62(12): p. 749-765.
- 49. Yilmaz D, Göktepe F, Göktepe O, Kremenakova D. Packing density of compact yarns. *Textile Research Journal*, 2007, 77(9): p. 661-667.

- 50. Azzi V, Tsai SW. Anisotropic strength of composites. *Experimental Mechanics*, 1965, 5: p. 283-288.
- 51. Madsen B, Hoffmeyer P, Thomsen AB, Lilholt H. Hemp yarn reinforced composites I. Yarn characteristics. *Composites Part A: Applied Science and Manufacturing*, 2007, 38: p. 2194–2203.
- 52. Harris B. *Engineering composite materials*, 1999. London: The Institute of Materials.
- 53. Naik N, Singh MN. Twisted impregnated yarns: Transverse tensile strength. *Journal of Strain Analysis for Engineering Design*, 2001, 36(4): p. 347-358.
- 54. Summerscales J, Dissanayake N, Virk AS, Hall W. A review of bast fibres and their composites. Part 2 Composites. *Composites Part A: Applied Science and Manufacturing*, 2010, 41(10): p. 1336-1344.
- 55. Pan N. Development of a constitutive theory for short fiber yarns: Part III: Effects of fiber orientation and bending deformation. *Textile Research Journal*, 1993, 63(7): p. 565-572.
- 56. Kelly A, Tyson WR. Tensile properties of fibre-reinforced metals: Copper/tungsten and copper/molybdenum. *Journal of the Mechanics and Physics of Solids*, 1965, 13(6): p. 329-350.
- 57. Aghdam M, Pavier MJ, Smith DJ. Micro-mechanics of off-axis loading of metal matrix composites using finite element analysis. *International Journal of Solids and Structures*, 2001, 38: p. 3905-3925.
- 58. Baley C, Perrot Y, Busnel F, Guezenoc H, Davies P. Transverse tensile behaviour of unidirectional plies reinforced with flax fibres. *Materials Letters*, 2006, 60: p. 2984-2987.
- 59. Kumar P. Mechanical behaviour of jute fibre and their composites. *Indian Journal of Technology*, 1986, 24: p. 29-32.
- 60. Ntenga R, Béakou A, Atéba JA, Ohandja LA. Estimation of the elastic anisotropy of sisal fibres by an inverse method. *Journal of Materials Science*, 2008, 43: p. 6206-6213.
- 61. Cichocki JF, Thomason JL. Thermoelastic anisotropy of a natural fiber. *Composites Science and Technology*, 2002, 62: p. 669-678.
- 62. Aly M, Goda IGM, Hassan GA. Experimental investigation of the dynamic characteristics of laminated composite beams. *International Journal of Mechanical & Mechatronics*, 2011, 10(3): p. 59-68.
- 63. BS EN ISO 527-4:1997 (BS 2782-3), Plastics Determination of tensile properties Part 4: Test conditions for isotropic and orthotropic fibre-reinforced plastic composites, 1997. British Standards Institution: London.
- 64. Chamis C. *NASA TN-D6696*, Design properties of randomly reinforced fibre composites, 1972. National Aeronautics and Space Administration: Washington DC.
- 65. Herrera-Franco P, Valadez-Gonzalez A. Mechanical properties of continuous natural fibre-reinforced polymer composites. *Composites Part A: Applied Science and Manufacturing*, 2004, 35(3): p. 339-345.
- 66. Charlet K, Jernot JP, Moussa G, Baley C, Bizet L, Breard J. Morphology and mechanical behaviour of a natural composite: the flax fiber, in *16th International Conference on Composite Materials (ICCM-16)*. 2007. Kyoto, Japan.
- 67. Hughes M, Carpenter J, Hill C. Deformation and fracture behaviour of flax fibre reinforced thermosetting polymer matrix composites. *Journal of Materials Science*, 2007, 42: p. 2499-2511.
- 68. Carpenter J, Miao M, Brorens P. Deformation behaviour of composites reinforced with four different linen flax yarn structures. *Advanced Materials Research*, 2007, 29-30: p. 263-266.

- 69. Halpin J, Tsai SW. *AFML-TR-67-423*, Environmental factors in composite design, 1967. Wright Aeronautical Laboratories: Dayton.
- 70. Halpin J, Kardos JL. The Halpin-Tsai equations: A review. *Polymer Engineering and Science*, 1976, 16(5): p. 344-352.
- 71. Thomason J, Carruthers J, Kelly J, Johnson G. Fibre cross-section determination and variability in sisal and flax and its effects on fibre performance characterisation. *Composites Science and Technology*, 2011, 71: p. 1008-1015.
- 72. Virk A. *Numerical models for natural fibre composites with stochastic properties*. PhD, 2010. University of Plymouth: Plymouth, UK.
- 73. d'Almeida J, Mauricio MHP, Paciornik S. Evaluation of the cross-section of lignocellulosic fibers using digital microscopy and image analysis. *Journal of Composite Materials*, 2012, 46(24): p. 3057-3065.
- 74. Thomason J, Gentles F, Brennan A. Natural fibre cross sectional area effects on the determination of fibre mechanical properties, in *15th European Conference on Composite Materials (ECCM-15)*. 2012. Venice, Italy.
- 75. Sinclair J, Chamis CC. Fracture modes in off-axis fiber composites. *Polymer Composites*, 1981, 2(1): p. 45-52.
- 76. Sinclair J, Chamis CC. *NASA TP-1081*, Mechanical behavior and fracture characteristics of off-axis fiber composites: I Experimental Investigation, 1977. NASA: Cleveland.